https://doi.org/10.5194/egusphere-2024-1290
Preprint. Discussion started: 5 June 2024

Evolution of biogeochemical Properties Inside Poleward Undercurrent Eddies in the Southeast Pacific Ocean

Lenna O. Ortiz[1,2,3], Oscar Pizarro[3,4], Marcela Cornejo-D'Ottone[5] and Boris Dewitte[6,7,8]

[1]Centro de Investigaciones en Ecosistemas de la Patagonia (CIEP), Coyhaique, Chile,
[2]Programa de Postgrado en Oceanografía, Departamento de Oceanografía, Facultad de Ciencias Naturales y Oceanográficas, Universidad de Concepción, Concepción, Chile,
[3]Millennium Institute of Oceanography, Universidad de Concepción, Concepción, Chile
[4]Department of Geophysics, University of Concepcion, Concepción, Chile,
[5]Escuela de Ciencias del Mar and Instituto Milenio de Oceanografía, Pontificia Universidad Católica de Valparaíso, Valparaíso, Chile,
[6]Centro de Estudios Avanzados en Zonas Aridas (CEAZA), Coquimbo, Chile
[7]Departamento de Biología Marina, Facultad de Ciencias del Mar, Universidad Católica del Norte, Coquimbo, Chile,
[8]LEGOS-CNRS/IRD/UPS/CNES, Toulouse, France

Correspondence to: Lenna O. Ortiz (lenna.ortiz@ciep.cl) and Oscar Pizarro (oscar.pizarro@imo-chile.cl)

Abstract. Oceanic eddies are ubiquitous features of the circulation through to be involved in transporting water mass properties over long distances from their source region. Among these is a particular type with a core within the thermocline with little signature visible from space. Despite their significance, their role in the ocean circulation remains largely undocumented from observations. This study characterizes the variations in internal biogeochemistry, disparities with external properties, and processes influencing the dissolved oxygen budget of Poleward undercurrent eddies (PUDDIES) during their transit to oceanic waters. Employing a high-resolution coupled simulation of the Southeast Pacific, we scrutinize eddy dynamics and biogeochemical processes associated with the nitrogen cycle, including characteristic mechanisms of Eastern Boundary Upwelling Systems (EBUS) such as denitrification. Our findings reveal that Puddies capture a biogeochemical signal contingent upon their formation location, particularly associated with the core of the Peru-Chile Undercurrent at the core of the Oxygen Minimum Zone (OMZ). While permeability at the periphery facilitates exchange with external waters, thereby modulating the original properties, the core signal retains negative oxygen (O_2) anomalies and positive anomalies of other biogeochemical tracers. These disturbances likely contribute to average properties that exceed the 90th percentile threshold in the open ocean, contrasting with the formation zone where they surpass 50th percentile levels. Suboxic cores are prevalent near the coast but decrease in abundance with distance from shore, giving way to a predominance of hypoxic cores, indicative of core ventilation during transit. The principal mechanism governing O_2 input into, or output from the eddy core entails lateral and vertical advection, with vertical mixing supplying O_2 to a lesser extent. Biological activity consumes O_2 for approximately 6 to 12 months more intensely the first 100 days, thereby facilitating the persistence of low O_2 conditions and extending the lifetime of biogeochemical anomalies within the core. The ammonium and nitrite depleted out of time in the eddy core with a decay rate greater than the nitrate and nitrous oxide, while these are accumulating in open sea. Our observations suggest that southern regions of the southeast Pacific OMZ undergo greater deoxygenation and nutrient enrichment due to Puddies compared to northern

https://doi.org/10.5194/egusphere-2024-1290
Preprint. Discussion started: 5 June 2024

regions. This underscores the significant role of Puddies in modifying biogeochemical conditions in the open ocean and in extending the boundaries of the Southern tip of the OMZ.

1 Introduction

Oxygen plays a fundamental role for life in the ocean, and numerous processes regulate its concentration in the water column. In subsurface waters (100-800 m depth), oxygen concentrations (O_2) decrease significantly due to the abundance and decomposition of organic matter and limited ventilation, leading to the formation of oxygen minimum zones (OMZ) in eastern boundary upwelling systems (EBUS; Wyrtki, 1962; Helly & Levin, 2004; Karstensen et al., 2008; Paulmier & Ruiz-Pino, 2009; Stramma et al., 2010). Under these conditions, heterotrophic metabolic processes prevail, dominated by activity of bacteria and archaea, resulting in significant shifts in biogeochemical cycles when O_2 fall below 20 µM.

The nitrogen cycle manifests in the oceans through various chemical species with different oxidation states. Outside the OMZ, where conditions are oxygenated, dinitrogen (N_2) is transformed into ammonium (NH_4^+), nitrite (NO_2^-), and nitrate (NO_3^-) through nitrification, with nitrous oxide (N_2O) formed as a byproduct. However, within the OMZ, where O_2 is depleted, nitrate becomes the primary oxidant, triggering denitrification. In this process, nitrate is reduced to gaseous forms (N_2 and N_2O), which can then be released into the atmosphere. This process has implications for primary production, carbon sequestration, and the release of N_2O into the atmosphere, a potent greenhouse gas (Goreau et al., 1980; Mantoura et al., 1993; Sarmiento & Gruber, 2006; Lam et al., 2009; Paulmier & Ruiz-Pino, 2009; Wright et al., 2012).

The southeast Pacific Ocean is the site of one of the most extensive and shallow OMZs (Paulmier & Ruiz-Pino, 2009), where anoxic conditions can even be observed (Ulloa et al., 2012). Several authors have determined the vertical and zonal extent of the OMZ, which exhibits significant seasonal variability, modulated both meridionally by subsurface currents towards the pole, and zonally by mesoscale processes (jets, eddies, fronts, filaments, etc.; Bettencourt et al., 2015; Chaigneau et al., 2011; Grados et al., 2016; Hormazabal et al., 2013; Morales et al., 2012; Stramma et al., 2013; Vergara et al., 2016; Pizarro-Koch et al., 2019). These processes result in changes in water mass properties, and together contribute up to a 25% reduction in O_2 volume during spring (Pizarro-Koch et al., 2019).

Furthermore, future projections suggest the expansion of these O_2 depleted zones through the global warming (Matear & Hirst, 2003; Stramma et al., 2010; Oschlies et al., 2018). Various mechanisms can potentially modify ventilation processes, leading to changes in subsurface water properties. The increase in sea surface temperature will affect O_2 solubility, and enhanced water column stratification will impact a range of biological processes that influence O_2 concentrations (Couespel et al., 2019; Keeling et al., 2010; Matear & Hirst, 2003; Oschlies et al., 2018; Schmidtko et al., 2017). The key role of turbulent dynamics in the functioning of OMZs is not considered in the current generation of climate models, limiting confidence in their projections, this is why understanding the role of mesoscale dynamics on the O_2 and carbon cycles in EBUS has been a major concern of the community.

https://doi.org/10.5194/egusphere-2024-1290
Preprint. Discussion started: 5 June 2024

'**P**oleward **u**ndercurrent e**ddies**' (Puddies) are types of subsurface or intrathermocline eddies characterized by coherent anticyclonic lenticular shaped vortices with cores located within the pycnocline and relatively homogenous interior waters (Dugan et al., 1982; McWilliams, 1985; Kostianoy and Belkin, 1989). Puddies originate in the Eastern Boundary Upwelling Systems (EBUS, Frenger et al., 2018) due to the interaction of the poleward-flowing current with the continental slope, generating submesoscale instabilities with anticyclonic vorticity, subsequently forming these characteristic mesoscale structures (Hormazabal et al., 2013; Combes et al., 2015, Molemaker et al., 2015; Thomsen et al., 2016; Contreras et al., 2019). These eddies represent 30-55% of the anticyclone eddies originating in the EBUS (Pegliasco et al., 2015; Combes et al., 2015) with cores that are warmer, saltier, O_2-depleted, and nutrient-enriched relative to surrounding waters (Collins et al., 2013; Hormazabal et al., 2013; Morales et al., 2012; Johnson and McTaggart, 2010). Therefore, Puddies can play a crucial role in transporting these water properties hundreds or thousands of kilometers offshore to subtropical gyres, contributing to the expansion of the OMZ beyond the coastal region (Frenger et al., 2018). Observations of low O_2 events in open ocean regions provide support for this idea (Lukas and Santiago-Mandujano, 2001; Johnson and McTaggart, 2010; Schütte et al., 2016b; Stramma et al., 2013, 2014; Karstensen et al., 2015), with further evidence of biogeochemical processes typically observed only in the OMZ, such as N_2O production (Cornejo et al., 2015; Arévalo-Martínez et al., 2016; Grundle et al., 2017) and nitrogen loss through denitrification (Altabet et al., 2012; Löscher et al., 2015). Additionally, the observed O_2 utilization rates within the eddy cores range from 0.29 to 44 nmol O_2 L^{-1} d^{-1}, which is up to 3 to 5 times higher than in the surrounding waters (Cornejo et al., 2015; Karstensen et al., 2015). There is evidence of harboring microbial communities and metabolisms associated with low-oxygen environments that persist even when the eddies enter highly oxygenated waters, a phenomenon known as the "stewpot effect" (Löscher et al., 2015; Frenger et al., 2018).

The Southeast Pacific (SEP) is characterized by extensive subsurface mesoscale eddy activity with radii ranging from ~25 to ~50 km and cores of ~500 m of vertical extent (Chaigneau et al., 2009; Hormazabal et al., 2013; Combes et al., 2015, Frenger et al., 2018). They transport a total volume of approximately 1 Sv (1 Sv = ~$1x10^6$ m^3 s^{-1}) westward with an average velocity of ~2 km d^{-1} (Hormazabal et al., 2013). The cores of these eddies exhibit homogenous salinity profiles (>34.5) and low O_2 concentrations (< 1.0 mL L^{-1}), linking them to Equatorial Subsurface Water (ESSW) transported poleward by the Peru-Chile Undercurrent (PCUC; Hormazabal, 2004; Colas et al., 2012; Hormazabal et al., 2013). Generally, the low values of O_2 in subsurface eddies is related to higher concentrations of nitrate, phosphate, and silicate (Czeschel et al., 2015). However, under suboxic conditions (O_2 < 20 μM), the prevailing anaerobic metabolism is denitrification, where nitrate is utilized as an electron acceptor, leading to increased production of NO_2^- and N_2O (Goreau et al., 1980; Mantoura et al., 1993; Lam et al., 2009; Wright et al., 2012). Within these eddies, various biogeochemical processes coexist that are highly sensitive to O_2 variations, while physical processes modulate biogeochemical patterns through mixing, submesoscale effects, or mass exchange with water masses from different origins through turbulent advection (José et al., 2017; Kartensen et al., 2017; Loveccio et al., 2022).

This complexity of processes involved during the life cycle of a Puddy, along with the lack of continuous in situ measurements, results in a limited understanding of nutrient recycling throughout their lifetime, and the

https://doi.org/10.5194/egusphere-2024-1290
Preprint. Discussion started: 5 June 2024

balance between processes controlling the rate of change of O_2 and nutrients. In the present study, we aim to characterize the internal biogeochemistry of eddies formed under various low-oxygen conditions in the SEP. We then analyze factors generating natural variability during the lifespan of bioelements associated with the nitrogen cycle during the trajectory of Puddies from the OMZ to better ventilated oceanic waters. Specifically, we document the evolution of water mass properties and processes inside puddies with contrasting initial characteristics in terms of O_2 concentration (suboxic versus hypoxic) in order to evaluate the role of these properties in OMZ maintenance. Our aim is also to fill in knowledge gaps in the biogeochemical dynamics of this type of eddy due to the lack of observational data, especially in the SEP. To quantify the changes that Puddies undergo as a result of their complex dynamics, we use a regional biogeochemical coupled model simulation. Two approaches are employed: 1) robust statistical analysis of contrasting water masses properties and rates within and outside the Puddies, and 2) case studies focusing on determining temporal changes in eddy properties along their trajectory. The organization of this study is as follows: Section 2 presents the details of the model and methods used for the identification and characterization of Puddies, Section 3 describes the biogeochemical characterization inside and outside the Puddies, temporal changes to the O_2 budget and the biogeochemical properties, Section 4 discusses the results and Section 5 presents the main conclusions and future projections.

2 Methods

2.1 Regional biogeochemical coupled model

We used a high-resolution, coupled physical-biogeochemical model simulation of the SEP that considers the main processes involved in the transformation of the water masses relevant to the OMZ variability and the dynamics of the Peru-Chile Undercurrent (PCUC). This current plays a significant role in generating Puddies and in the southward extension of the OMZ in the Peru-Chile Eastern Boundary Upwelling System (EBUS).

The physical dynamics were simulated using the Regional Ocean Modelling System (ROMS), a regional ocean circulation model that solves the primitive equations with free surface and sigma coordinates (Shchepetkin and McWilliams 2005, 2009). ROMS was coupled with the biogeochemical model BioEBUS, specifically developed for Eastern Boundary Upwelling Systems (EBUS) and based on the nitrogen cycle using $N_2P_2Z_2D_2$ model formulation (Koné et al., 2005; Gutknecht et al., 2013a). We adopted the same configuration as specified in several other studies in the region (Dewitte et al., 2012; Montes et al., 2014; Vergara et al., 2016; Pizarro-Koch et al., 2019) using a spatial resolution of 1/12°, 37 vertical levels, with outputs every three days, suitable for resolving mesoscale features. The overall domain covers the latitudinal range of 12°N to 40°S from the coast to 95°W, although the present study focuses on latitudes off the coast of Chile between 20° and 40°S (Figure 1a). The simulated period was from 2000 to 2008.

https://doi.org/10.5194/egusphere-2024-1290
Preprint. Discussion started: 5 June 2024

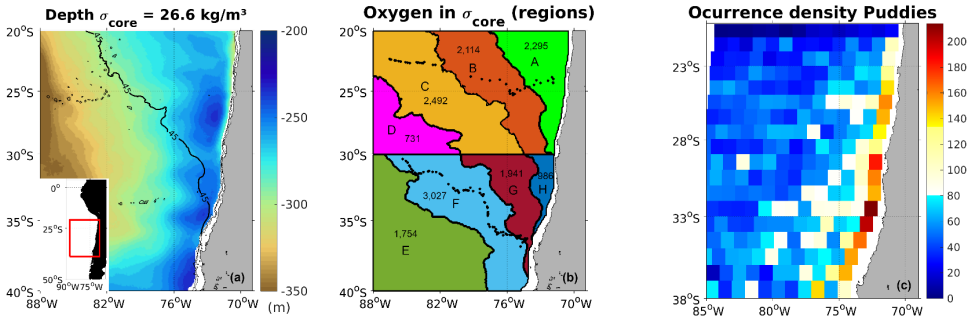

Figure 1. Depth of the OMZ core, modeled dissolved O_2 climatology offshore of the Chilean coast, and spatial distribution of the occurrence density of the Puddies identified over the nine year period. (a) The OMZ core was considered as being in the isopycnal layer 26.6 kg/m^3 (defined with S_{core} layer; see Section 2.2). The study area covers 20 - 40ºS and from the coast to 88ºW. The black contour shows the traditional OMZ limit ([O_2]=1mL/L or ~ 45 µM) at -300 m. Black lines represent isobaths of -1000 m and -500 m. (b) Subregions are defined by the following O_2 contours using the S_{core} layer: Region A (O_2 < 20 µM), Region B and Region H (20 µM < O_2 < 45 µM), Region C and Region G (45 µM < O_2 < 90 µM), Region D and Region F (90 µM < O_2 < 120 µM) and Region E (120 µM < O_2). Yellow dots indicate the path of the tracking of two Puddies for the case studies. Numbers are the total profiles counted in each region. The same colors will be used in the following figures to refer to the subregions. (c) Occurrence density (colormap) is quantified by the total number of Puddies identified in each 1°x1° area for each snapshot (Δt = 3 days), with the possibility that the same eddy may be counted more than once if remaining in the same area. Numbers refer to the total occurrence density by region.

The model uses atmospheric forcing data from NCEP-NCAR (2.5° x 2.5°, Goubanova et al., 2011). Latent heat flux and other variables –for estimating other air-sea fluxes– such as air temperature and humidity are provided by monthly climatology with a resolution of 1° x 1° from COADS (da Silva et al., 1994). The boundary conditions for temperature, salinity, and horizontal velocity were provided by the SODA 1.4.2 reanalysis (Smith et al., 1992). The BioEBUS model consists of 12 compartments interacting through advection-diffusion equations and source-minus-sink (SMS) processes. The considered components include inorganic dissolved nutrients (NO_3^-, NO_2^-, and NH_4^+), large and small phytoplankton ("small" representing nanophytoplankton; mainly small flagellates between 2 and 20 µm and "large" representing microphytoplankton; mainly diatoms between 20 and 200 µm), large and small zooplankton ("small" representing microzooplankton; mainly heterotrophic ciliates between 20 and 200 µm, and "large" mesozooplankton; mainly copepods between 200 µm and 2 mm), and detritus (small and large). Dissolved organic nitrogen (DON) was considered following the formulation of Dadou et al. (2001, 2004) and Huret et al. (2005), O_2 including its ocean-atmosphere interaction according to Peña et al. (2010) and Yakushev et al. (2007), and the production of N_2O using the parameterization of Suntharalingam et al. (2000, 2012). The boundary and initial conditions for the BioEBUS model were obtained from the CARS2006 climatology (CSIRO Atlas of Regional Seas) for O_2 and NO_3^-, with constant vertical profiles adopted for NH_4^+, NO_2^-, and dissolved organic nitrogen (DON) (based on Koné et al., 2005). Phytoplankton biomass was estimated based on chlorophyll concentration (Chl-a) –obtained from SeaWiFS climatological satellite data– and then extrapolated vertically using the method of Morel and Berthon (1989). Detailed information on simulation

https://doi.org/10.5194/egusphere-2024-1290
Preprint. Discussion started: 5 June 2024

and validation of the physical model (ROMS) is given by Dewitte et al. (2012) and Vergara et al. (2017). The parameter configuration of BioEBUS is the same as used in Montes et al. (2014) for the Peruvian region, Vergara et al. (2016) for the northern region of Chile, and Pizarro-Koch et al. (2019) for the central-southern region of Chile.

The time rate of change of the concentration of each component is governed by the advection-diffusion equation (Equation 1, see Gutknecht et al., 2013a). For instance, the O_2 balance is given

$$\frac{\partial O_2}{\partial t} = -\nabla \cdot (uO_2) + K_H \nabla^2 O_2 + \frac{\partial}{\partial z}\left(K_z \frac{\partial O_2}{\partial z}\right) + SMS(O_2) \quad (1)$$

where $u = (u, v, w)$ represents the fluid velocity, with component u for zonal, v for meridional, and w for vertical. The first term on the right-hand side represents the advection (ADV = $-\nabla \cdot (uO_2)$), which is an scalar, but can also be decomposed in the sum of zonal (XADV = $-u\frac{\partial O_2}{\partial x}$), meridional (YADV = $-v\frac{\partial O_2}{\partial y}$), and vertical (VADV = $-w\frac{\partial O_2}{\partial z}$) components. The second and third terms correspond to horizontal (HMIX) and vertical (VMIX) diffusion, where K_H is the horizontal eddy diffusion coefficient (set to 100 $m^2\ s^{-1}$ in this version of the model), and K_z is the turbulent diffusion coefficient calculated using the K-profile parameterization mixing scheme (Large et al., 1994). The last term $SMS(O_2)$ represents the effect of sources and sinks associated with the relevant biogeochemical processes. For O_2, the source process is primary production, and sink processes include remineralization, nitrification, and zooplankton excretion.

2.2 Characterization of the study area

The study area extends from 20º to 40ºS and from the Chilean coast to 88ºW. In this region the OMZ core (O_2 < 45 μM or ~ 1 mL/L) is centered at a density surface of σ_θ = 26.6 kg m^{-3} whose depth varies, being shallower in the coastal area and deepening in the oceanic region (Figure 1a). Near the slope, a deepening in S_{core} is observed north of 30°S, where the slope is narrower. South of 30°S, it widens, as indicated by the 1000 m and 500 m depth isobaths.

All variables were interpolated from the original sigma vertical coordinate to depth every 5 meters from 800 m to the surface. In the deep ocean (~4000 m depth) typically 13 of the 37 vertical levels fall within this depth range. Two main zones were considered: the northern zone (20º–30ºS), where the OMZ is zonally wider and characterized by suboxic conditions (O_2 < 20 µM); and the southern zone (30º - 40°S), where the OMZ is mostly hypoxic (O_2 < 45 µM) and much narrower (Figure 1b). Subsequently, we adopted additional criteria to subdivide those regions, using ranges that define the various metabolic niches for organisms: region A with O_2 < 20 µM, region B and H with 20 µM < O_2 < 45 µM, region C and G with 45 µM < O_2 < 90 µM, region D and F with 90 µM < O_2 < 120 µM and region E with 120 µM < O_2. This subdivision was based on O_2 concentrations observed on a density surface that represent the core of the Pudies (S_{core} = 26.6 kg m^{-3}, the S_{core} depth is shown in Figure 1a).

The region within the first ~100 km off the coast was considered as a formation zone for Puddies where a large number of surface and subsurface eddies are typically generated (e.g., Chaigneau et al., 2009; Figure

https://doi.org/10.5194/egusphere-2024-1290
Preprint. Discussion started: 5 June 2024

1c). Along the coast, approximately 1° of latitude x 1° longitude boxes were selected to characterize the biogeochemical properties of the source water that the Puddies eventually enclose upon formation.

2.3 Definition of "mean state" and mesoscale contribution

To estimate the physical and biogeochemical perturbations from the mean field associated with the eddies, we use a Reynolds-like decomposition, which for the field of NO_3^- concentration is written as follows Eq. (2):

$$NO_3(x,y,z,t) = \underline{NO_3} + NO_3'(x,y,z,t) \quad (2)$$

where $\underline{NO_3}\ (x,y,z)$ is the "mean state" of NO_3^- over the period 2000-2008, with fluctuations of this "mean state" corresponding to $NO_3'(x,y,z,t)$. Similarly, for other variables involved, $\underline{S}$, $\underline{N_2O}$, etc., denoted the "mean state", whereas S´, N_2O´ etc., correspond to anomalies, which includes eddy fluctuations and changes associated with annual and interannual variability. This decomposition method was used for all variables analyzed in each subregion of study. To evaluate the impacts of the Puddies on the various fields, we used an algorithm to identify subsurface eddies (See details in Section 2.5) and then compared the perturbed fields inside the Puddies with the total field. This procedure is further explained in section 2.6.

2.4 Calculation of AOU, ΔNO_3^- and ΔN_2O

The apparent oxygen utilization (AOU), NO_3^- production (ΔNO_3^-), and N_2O production (ΔN_2O) provide an estimate of how much has been produced/consumed by biological processes since the water mass was formed. These estimates are associated with the time the water mass has spent without coming into contact with the ocean surface or being ventilated.

The AOU calculation was derived from the García & Gordon (1992) algorithm, based on the O_2 saturation concentration at any temperature and salinity, and using the following Eq. (3):

$$AOU = [O_2]_{sat} - [O_2]_{obs} \quad (3)$$

The N_2O saturation (ΔN_2O) was calculated using the Gruber & Sarmiento (2002) methodology and the following relationship Eq. (4):

$$\Delta N_2O = [N_2O]_{obs} - [N_2O]_{sat} \quad (4)$$

NO_3^- production (ΔNO_3^-) is defined as follows Eq. (5):

$$\Delta NO_3^- = [NO_3^-]_{obs} - [NO_3^-]_{preformed} \quad (5)$$

The value of $[NO_3^-]_{preformed}$ in subsurface waters considered for the above calculation was that of Equatorial Subsurface Water (ESSW) in all regions except E, where the value for Antarctic Subsurface Water (SAAW)

https://doi.org/10.5194/egusphere-2024-1290
Preprint. Discussion started: 5 June 2024

was taken from Llanillo et al. (2012). The assessment of the modeled surface NO_3^- is provided in Appendix 1.

2.5 Puddy Identification and Tracking

For the identification of Puddies, the algorithm proposed by Faghmous et al. (2015) (see: https://www.nature.com/articles/sdata201528) was adapted to deal with subsurface eddies that have a weak dynamical signature at the surface of the ocean. The original algorithm is based on the presence of local extreme values (minimum in the case of cyclonic eddies and maximum in the case of anticyclonic eddies, considering a neighborhood defined a priori around it) of sea level anomalies (SLA). Because the SLA signal from subsurface eddies may be rather weak or absent, the present study used anomalies in the layer thickness (δh). This layer is bounded by the density surfaces S_{upper} = 26.0 kg m^{-3} and S_{lower} = 26.9 kg m^{-3}. Thus, positive anomalies ($\delta h > 0$) indicate the presence of subsurface anticyclonic eddies due to their convex shape (for our case, Puddies). When δh is at its maximum (δh_{max}), the largest closed contour around the geographical location of δh_{max} is considered as the edge of the eddy, as δh_{max} is associated with the center of the eddy and the points contained within the eddy edge are the body of the eddy (Faghmous et al., 2015). Starting from δh_{max}, a gradual decrease of 0.1 m was used to establish the size and amplitude of the eddy. Only eddies that reached a minimum horizontal area of 30 grid points (A_{min}~1.95x10^9 m^2, equivalent to a radius of ~ 25 km) were considered here because eddies below that threshold size are not well identified. For the present analysis, only eddies that did not exceed a radius of 150 km were considered. The identification of eddies was conducted every three days over the entire period. Subsequently, all δh_{max} positions were classified by subregion and in 1°x1° cells for their enumeration (Figure 1b, 1c) and for characterizing the average properties of these Puddies (statistical analyses are shown in section 3).

For the case studies, two Puddies formed in zones with contrasting biogeochemical properties (i.e., zones A and G) were selected and followed. The algorithm kept track of both eddies, although tracking was lost at certain times. In the case of the eddy formed in region A, the track was lost for up to 87 days (29 time steps), whereas for the eddy formed in region G, the maximum number of days without tracking was 27 days (9 time steps). Long gaps were manually corrected with δh_{max} search, the verification of the trajectory was carried out under visual inspection of the vertical sections of vorticity fields and O_2 contours. Finally, short gaps (shorter than 3-time steps) in the Puddy trajectories were filled using linear interpolation.

2.6 Compound Formation

2.6.1 Average Profiles

To understand the typical conditions within Puddies identified in the formation zone and each subregion, average profiles were constructed as follows: i) all eddy centers (i.e., δh_{max} positions) were classified according to the regions defined in Figure 1 ii) for each eddy center, vertical profiles were extracted between

https://doi.org/10.5194/egusphere-2024-1290
Preprint. Discussion started: 5 June 2024

the density surfaces S_{upper} and S_{lower} for all variables, for each corresponding region iii) then, these profiles were time-averaged to obtain typical profiles for each variable. The analysis of these results is presented in sections 3.1 and 3.2.

2.6.2 Puddy evolution

As a case study, we characterize the evolution of several variables within two Puddies. The selected eddies exhibited a long trajectory toward the open ocean with a lifetime > 1 year. For these Puddies, we estimate characteristics inside the entire eddy volume as follows: i) an average radius (r_{mean}) during its entire trajectory was calculated, ii) a circular polygon (eddy mask) with a r_{mean} was drawn around the Puddy center to extract all the grid points within the circumference. The same mask was applied to all depths (every 5 meters) creating a cylinder between S_{upper} and S_{lower}. From the total volume enclosed by the cylinder, an average vertical profile was obtained at each time step for each variable. The temporal evolution of these two Puddies is presented in sections 3.4 and 3.5.

2.7 Calculation of percentiles

To quantify the significance of the internal contribution of Puddies compared to the average state, a random sampling of positions (> 200) was conducted for each region to extract variables in the S_{core} at approximately 100 different time points. Subsequently, the 50th, 75th, and 90th percentiles (P50, P75, P90) were calculated from these samples and compared to results obtained in Section 3.2.3 (Table 4).

3 Results

3.1 Contrasting biogeochemical characteristics inside and outside the Puddies

Over the 9-year study period in the simulated study region (Figure 1), a mean of approximately 14 Puddies were observed each day, resulting in a total of ~15,340 Puddy profiles identified over the entire study period. If the same eddy remained within the same 1°x1° grid area, it was counted multiple times (using a 3-day time step) until the center of the eddy moved to an adjacent 1°x1° grid. The area with the highest density of identified Puddy profiles was concentrated in the coastal region (2,548), within the first ~100 km from shore, with the maximum abundance noted between 29º – 35ºS (Figure 1c). It should be noted that the number of eddies in the coastal region may be slightly overestimated by our adopted algorithm due to difficulties in distinguishing between perturbations of the density surfaces generated by eddies, coastal upwelling events, coastally trapped waves or meanders of the coastal currents.

To assess the impact of Puddies along the coastal strip, we evaluated the mean distribution of several variables (salinity, O_2, NO_3^-, NO_2^-, NH_4^+, and N_2O) in coastal boxes of approximately 1°X1° between 20°S and 38°S, and between the isopycnal surfaces S_{upper} and S_{lower} that define the OMZ core in the model (see

https://doi.org/10.5194/egusphere-2024-1290
Preprint. Discussion started: 5 June 2024

details in Section 2.6.1). Then, we calculated the mean profiles of these variables in the center of the Puddies observed in each coastal box, and estimated anomalies of the profiles with respect to the general mean profile of the corresponding box (Figures 2, see also Figure S1 in the supplementary material).

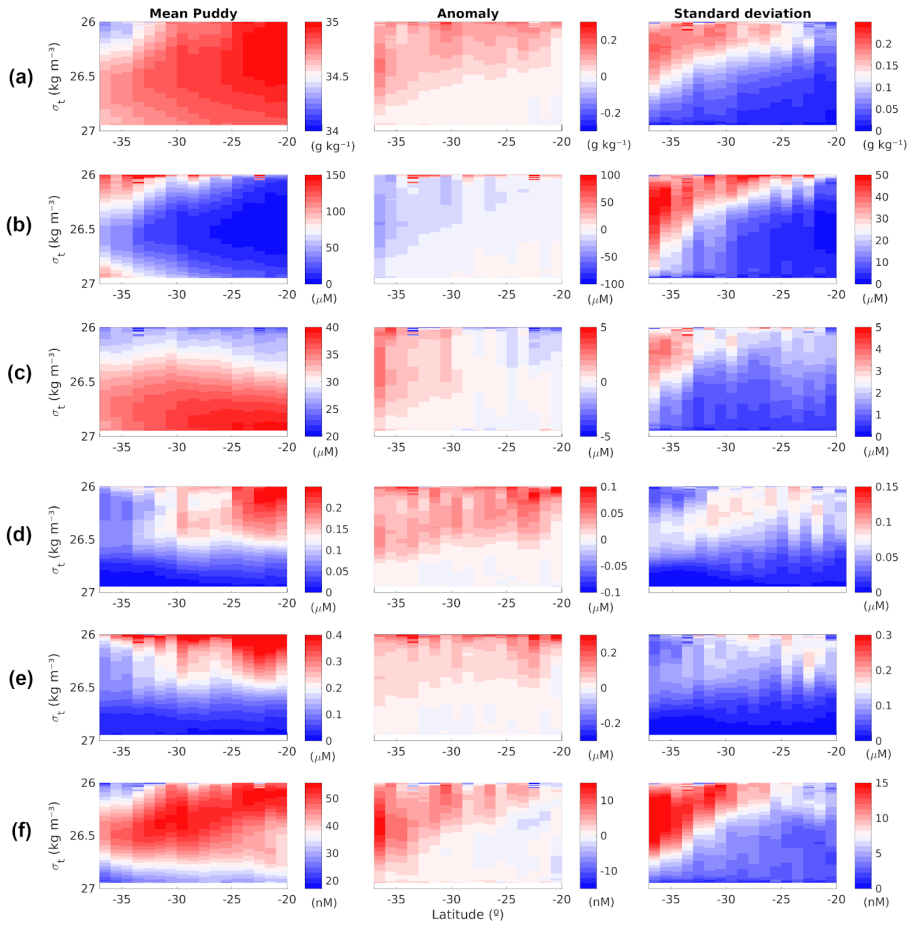

Figure 2. Average vertical profiles, standard deviation, and anomalies associated with biogeochemical features within the center of the Puddies over the first ~100 km from the slope. Eddies' average profiles (left boxes) were obtained by calculating the mean of total profiles identified during nine years in 1°x1° boxes along the coast between the isopycnal layers s_{upper} and S_{lower} (See Methods 2.2, 2.3, 2.6.1). The standard deviation (right boxes) is interpreted as the variability of the properties existing at the center, and the anomalies (middle boxes) were calculated by removing the mean state related to the same volume element. (a) absolute salinity, (b) O_2, (c) NO_3^-, (d) NO_2^-, (e) NH_4^+, and (f) N_2O.

Meridional changes in water properties along the coastal strip impact the initial properties of the Puddies. In the northern sector (between 20°S and 30°S), the waters are warmer, more saline, and have lower O_2 , with

https://doi.org/10.5194/egusphere-2024-1290
Preprint. Discussion started: 5 June 2024

higher concentrations of NO_2^- and NH_4^+ (Figures 2e and 2d); whereas towards the south (south of 30°S), these characteristics generally show the opposite tendency, consistent with the water properties observed within Puddy cores. However, NO_3^- and N_2O show maximum levels in the central region (near 30°S) (Figures 2c and 2f), where eddies with the highest N_2O concentrations are also observed. Oxygen levels were higher at the upper and lower limits of the OMZ (i.e., near σ_θ = 26.3 kg m^{-3} and σ_θ = 26.7 kg m^{-3}) and remained relatively low in the OMZ core (σ_θ ~26.5 kg m^{-3}). Both NH_4^+ and NO_2^- anomalies generated by the Puddies showed maximum values in the upper limit of the eddy cores (near σ_θ = 26.3 kg m^{-3}) and were fairly uniform along the coastal strip, except between 22º - 24ºS and the north-central region, which showed slightly higher anomalies (Figures 2d).

3.2 Biogeochemical characteristics inside the offshore Puddies

From the total of 15,340 Puddies profiles identified in the study region (more details in Section 2.2), the number recorded for each region varied (Table 2, Figure 1b). The number presented in Table 2 were used as sample size for different statistical estimation (see below). General characteristics associated with each subregion are detailed in Table 1.

Table 1. General characteristics of the study subregions.

Regions	Number of pixels	Depth S_{upper} (m)		Depth S_{lower} (m)		Mean thickness (m)
		Min	Max	Min	Max	
A	5550	-140	-50	-510	-435	377
B	7632	-190	-85	-465	-435	313
C	10202	-240	-130	-495	-435	280
D	4016	-250	-190	-500	-450	255
E	11709	-240	-145	-485	-380	240
F	9349	-235	-85	-485	-405	285
G	4190	-195	-90	-480	-420	308
H	1323	-130	-65	-485	-440	365

https://doi.org/10.5194/egusphere-2024-1290
Preprint. Discussion started: 5 June 2024

3.2.1 Conditions of Suboxia and Hypoxia in the Oceanic Puddies

We assessed the number of Puddies exhibiting suboxia and hypoxia in each region by identifying the predominant type of low-oxygen cores in coastal and oceanic regions. The percentage of Puddies exhibiting hypoxia ($O_2 < 45$ µM) and suboxia ($O_2 < 20$ µM) was determined by classifying the range of O_2 concentrations observed in the center of the eddies. The presence of Puddies with these characteristics in the more remote regions was quantified (regions C, D and E in Table 2).

Table 2. Percentage of total identified Puddies showing suboxic ($O_2 < 20$ µM) and hypoxic ($O_2 < 45$ µM) cores within each region.

Regions	Total profiles	Mean thickness (m)	Suboxic cores (%)	Hypoxic cores (%)
A	2,295	475	100	0
B	2,114	317	70	30
C	2,492	317	13.8	60
D	731	335.6	< 1	3
E	1,754	445	0	0.1
F	3,027	505	< 1	9
G	1,941	540	9.3	60
H	986	551.6	30	70

3.2.2 Relationship between internal biogeochemical components

Each water mass acquires characteristics through physical and biochemical processes, producing particular relationships between the physicochemical variables. Low O_2 waters are closely related to relatively salty ESSW waters. In our study region, this water mass is located between the low salinity and relatively well-ventilated water masses (i.e., ESPIW above and AIWW below). Thus, salinity and O_2 show a linear inverse correlation between the upper and lower oxyclines that delimit the OMZ. Nevertheless, the occurrence of

https://doi.org/10.5194/egusphere-2024-1290
Preprint. Discussion started: 5 June 2024

biogeochemical processes can disrupt this relationship. Therefore, it is useful to quantify which regions show these nonlinear biogeochemical processes in the context of a hypothesis that a linear relationship between O_2 and salinity corresponds to an aging of the water mass due to lack of ventilation. A nonlinear relationship would imply the presence of other processes such as denitrification. Linear regression was performed between absolute salinity, O_2, and AOU on the S_{core} surface, where AOU provides a measure of the apparent O_2 consumption since the ESSW formation (Table 3).

Table 3. Linear regression between $\underline{AOU}$, $\underline{O_2}$ (μM) and absolute salinity (g kg^{-1}) within the S_{core} (σ_θ = 26.6 kg m^{-3}) layer for each subregion.

Regions	$\underline{AOU}/\underline{S}$			$\underline{O_2}/\underline{S}$		
	R^2	**Slope**	**Intercept**	**R^2**	**Slope**	**Intercept**
A	0.88	112.5±0.57	-3664.6±21	0.92	-142±0.6	4963.5±20.1
B	0.85	199.2±1	-6685.2±33.5	0.88	-229±0.9	7998.6±33.4
C	0.92	301.8±0.8	-10252±28.8	0.94	-332.4±0.8	11590±28.6
D	0.94	457.45±1.7	-15642±59.6	0.95	-488.6±1.7	16999±59.2
E	0.39	302.8±3.4	-10308±117.9	0.45	-339.9±3.4	11872±117.3
F	0.44	202±2.3	-6807.9±80.5	0.53	-236.6±2.3	8281.6±79.8
G	0.95	294.5±1	-9989.3±36.2	0.96	-327.1±1	11396±36
H	0.98	200.8±0.7	-6737±25.2	0.99	-232±0.7	8097±25.6

Oxygen and AOU exhibited a strong linear relationship with absolute salinity ($R^2 > 0.85$) in regions where there is a greater contribution from ESSW (Regions A, B, C, D, H, G). The correlation coefficients varied between 112.5 and 457.45, whereas regions F and E did not show a linear relationship ($R^2 < 0.45$), which can be explained by the influence of SAAW and AAIW waters mixing properties with ESSW (Figure S2a, Table 3). Region H ($R^2 = 0.99$) showed the strongest relationship, which decreased in regions A and B ($0.85 < R^2 < 0.9$) where denitrification processes are more evident.

On the other hand, the asymptotic behavior of NO_2^- was similar to that of NH_4^+, occurring when $O_2 < 45$ μM (regions: A, B, and H) and tending towards undetectable in regions where $O_2 > 45$ μM (Figure 3c, S3). Nitrous oxide decreased under suboxic conditions, increased under hypoxic conditions in regions G and H,

https://doi.org/10.5194/egusphere-2024-1290
Preprint. Discussion started: 5 June 2024

but decreased in regions B and C under similar O_2 conditions to those observed in G and H regions (Figure 3d).

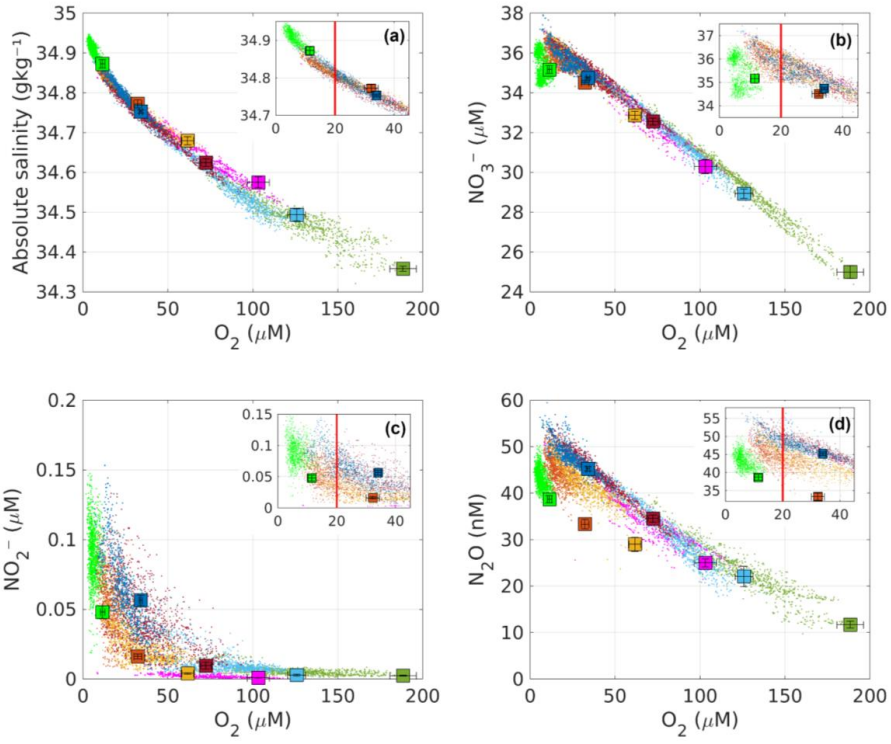

Figure 3. Relationship between O_2 concentration and the absolute salinity, NO_3^-, NO_2^-, and N_2O at the S_{core} layer for all identified Puddies. Color dots corresponding to the mean property at the core of Puddy (section 2.5) are contrasted with the mean state (color squares, section 2.3). The colors used for the regions are the same as Figure 1b. Vertical error bars show the y-axis standard deviation, whereas the horizontal error bars are the standard deviation of O_2. The smaller box shows a magnification of the larger box for hypoxic and suboxic conditions, the red line indicates the threshold of O_2 = 20 μM.

3.2.3 Differences between biogeochemical properties inside and outside Puddies

To understand the biogeochemical impacts of eddies in oceanic waters, the values found in the core of the Puddies were compared with the "mean conditions" of each region (Figures 3, 4, S2b, S2c, S2d; see Methodology in sections 2.5, 2.6.1). The presence of Puddies manifests a change in layer thickness (δh) with respect to the average δh by region (Table 1 and 2) with greater contrast observed away from the coast in the south. Values of $\underline{AOU'}$, $\underline{\Delta NO_3'}$ and, $\underline{\Delta N_2O'}$ observed inside the Puddies were higher than $\underline{AOU}$, $\underline{\Delta NO_3}$ and $\underline{\Delta N_2O}$ observed outside (Table 4) confirming that eddies maintain hypoxic or suboxic cores that impact

https://doi.org/10.5194/egusphere-2024-1290
Preprint. Discussion started: 5 June 2024

regions farther offshore, as shown in the Section 3.2.2 (Table 2). Nonlinear biogeochemical processes observed in the OMZ (Section 3.2.2) were commonly observed in the Puddies that arrived in regions C and G (Figure 3), but less frequently in those arriving in regions D, E, and F. Additionally, in the hypoxic/suboxic regions where these nonlinear processes are usually more pronounced, signals were intensified within the Puddies (Regions A, B, and H; Figure 3). In general, in the coastal areas (A and H regions), Puddies exhibited an increment of > 0.15 salinity, 1 – 4 µM NO_3^- (+2.25 – 3.4%), up to 0.05 µM NH_4^+ similar to NO_2^- (+12.5 – 83%), and 3 – 12 nM N_2O (+8.5 – 15%) associated with an increase of the 7 – 9 µM AOU (+2.5 – 4%) higher than the "mean conditions" (Table 2). These anomalies were close to the P75 (P90 for the salinity) indicating a significant elevation over mean state contributed by the Puddies (Table 5). Offshore, the contrast over mean state was greater, reaching >300% of NH_4^+ (region F), +50% of NO_3^- (region E), >85% N_2O (region F), 30 - 60% for AOU and 0.17 for salinity (Table 4). These values exceed the P90 in region E and C, and P75 in other oceanic regions. Clearly, the perturbations to the mean state contributed by Puddies in open sea is more significant than near the coast (Table 5). Salinity and biogeochemical tracers decrease as the core becomes more oxygenated (Figures 3a, 4a; Table 4).

Table 4. Average values of AOU (µM), absolute salinity (g/kg), NH_4^+ (µM), ΔNO_3^- (µM), and ΔN_2O (nM) inside and outside the Puddies (mean state) on the S_{core} surface (σ_θ = 26.6 kg m^{-3}). $\underline{()}$ indicate the mean value of the corresponding variable in the corresponding region, while $\underline{()'}$ is the value of the variable inside the Puddies (see Methods 2.3 and 2.6.1).

Regions	$\underline{AOU}$	$\underline{AOU'}$	$\underline{S}$	$\underline{S'}$	$\underline{NH_4}$	$\underline{NH_4'}$	$\underline{\Delta NO_3}$	$\underline{\Delta NO_3'}$	ΔN_2O	$\underline{\Delta N_2O'}$
A	259.8±1.13	265.0±1.91	34.70±0.011	34.87±0.010	0.06±0.007	0.11±0.026	17.85±0.11	18.3±0.65	28.79±0.96	33.4±2.15
B	241.4±2.22	256.6±4.85	34.60±0.011	34.77±0.010	0.02±0.003	0.07±0.025	17.1±0.1	18.7±0.51	23.5±0.98	34.9±3.13
C	214.9±3.08	241.0±11.98	34.50±0.009	34.68±0.010	0.007±0.0005	0.03±0.012	15.55±0.19	17.9±0.93	19.5±1.34	31.5±4.1
D	177.2±6.21	205.5±16.16	34.40±0.013	34.58±0.013	0.002±0.00008	0.005±0.002	13.2±0.31	15.2±1.17	14.6±0.88	22.2±4.41
E	100.6±9.11	159.1±24.1	34.18±0.013	34.36±0.006	0.006±0.0008	0.01±0.003	7.9±0.85	12.1±1.85	0.7± 0.8	12.5±5.73
F	158.7±4.73	201.5±20.75	34.32±0.021	34.49±0.015	0.007±0.001	0.03±0.016	11.9±0.32	15.0±1.6	11.2±2.44	21.7±7.3
G	208.1±2.96	236.8±15.37	34.45±0.012	34.62±0.009	0.02±0.003	0.06±0.028	15.4±0.21	17.6±1.15	24.5±0.97	33.8±5.52
H	240.4±0.97	249.8±7.43	34.58±0.004	34.75±0.004	0.08±0.005	0.09±0.028	17.7±0.07	18.4±0.6	34.65±0.47	37.8±2.95

https://doi.org/10.5194/egusphere-2024-1290
Preprint. Discussion started: 5 June 2024

The AOU/ΔNO_3^- ratio allows us to quantify the remineralization of organic matter through aerobic processes, which is determined by the Redfield ratio ($R_{N/O}$; 16/138 = 0.11; Redfield et al., 1963). Changes in this relationship indicate the presence of other biological processes that contribute/consume nitrogen in a system, such as nitrogen fixation (ΔNO_3^- /AOU > $R_{N/O}$) and denitrification (ΔNO_3^- /AOU < $R_{N/O}$). On the other hand, the ΔN_2O/AOU ratio provides a measure of N_2O accumulation, so that a high ΔN_2O/AOU is associated with the denitrification process (Sarmiento & Gruber, 2006).

We observed a ΔNO_3^- /AOU < $R_{N/O}$ inside and outside the Puddies (Figure 4d), indicating a deficit of NO_3^- and high O_2 consumption due to the high remineralization in subsurface waters. The ratio is higher in the suboxic region (Region A, Figure 4d) with an AOU:ΔNO_3^- = 15:1, while in the other regions this signal of old and poorly ventilated waters also extends, albeit in different proportions (Table 4). When $\frac{\Delta NO'_3}{AOU'} < \frac{\Delta NO_3}{AOU}$, it must be the case that $AOU' > AOU$ or $\Delta NO'_3 < \Delta NO_3$. Since the second assumption is not met, it follows that $AOU' > AOU$ (Table 4). However, in regions B and C, $\Delta NO'_3 < AOU'$, indicating that $\Delta NO'_3 > \Delta NO_3$ or $AOU' < AOU$. Given that $AOU' > AOU$, it must have occurred that $\Delta NO'_3 > \Delta NO_3$, so the production of NO_3^- was greater in the Puddies found in these regions compared to others (Table 4). On the other hand, it holds that $\frac{\Delta N_2O'}{AOU'} > \frac{\Delta N_2O}{AOU}$. Since $AOU' > AOU$, it also follows that $\Delta N_2O' > \Delta N_2O$, therefore the production of N_2O was proportionally larger than O_2 consumption in the Puddies (Table 4). Note that although in regions H and G the eddies exhibited the highest values of $\frac{\Delta N_2O'}{AOU'}$, $\frac{\Delta N_2O}{AOU}$ was also high (Figure 4d). Additionally, the variability of physicochemical conditions in the core increased with distance from the coast and with oxygenation.

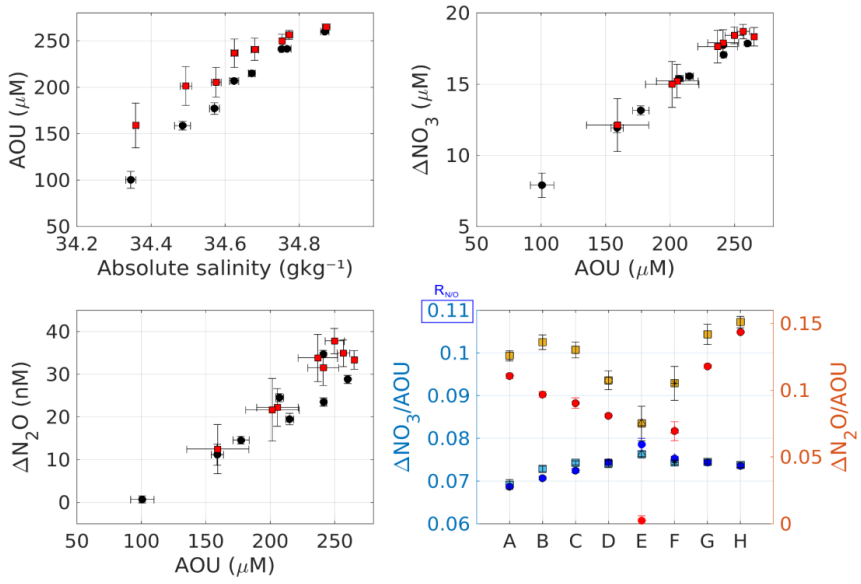

https://doi.org/10.5194/egusphere-2024-1290
Preprint. Discussion started: 5 June 2024

Figure 4. Mean properties and ratios of the average Puddy and mean state for each region. Relations between AOU and (a) absolute salinity, (b) ΔNO_3^-, and (c) ΔN_2O. (d) Ratios of ΔNO_3^-/AOU and Δ/AOU (blue/yellow squares (Puddy), blue/red circles (mean state)). (a-c) Values estimated inside eddies are shown in black squares and the average for the whole subregion by red squares. Vertical error bars show the y-axis standard deviation, whereas the horizontal error bars are the x-axis standard deviation. (d) Values estimated inside eddies are shown in squares and the mean state in circles. The error bars show ½ of the corresponding standard deviations. The average was calculated for the S_{core} layer (see Section 2.3, 2.5). The Redfield ratio ($R_{N/O}$ = 0.11) is shown on the left axis.

Table 5. Percentiles 50th, 75th, and 90th (P50, P75, P90) of AOU (µM), absolute salinity (g/kg), NH_4^+ (µM), ΔNO_3^- (µM), and ΔN_2O (nM) on the S_{core} surface (σ_θ = 26.6 kg m^{-3}). The profiles were obtained from random samples (# pro.) for each region.

Reg	# pro.	AOU			S			NH_4^+			ΔNO_3^-			ΔN_2O		
		P50	P75	P90	P50	P75	P90	P50	P75	P90	P50	P75	P90	P50	P75	P90
A	1246	257	266	269	34.72	34.77	34.79	0.06	0.12	0.17	18.08	18.47	18.87	32.48	35.6	39.56
B	1474	244	254	261	34.6	34.64	34.69	0.009	0.019	0.048	16.98	17.92	18.61	25.28	32.24	37.78
C	2882	213	227	241	34.49	34.54	34.58	0.002	0.005	0.01	14.73	16.12	17.41	16.78	23	30.8
D	627	161	182	210	34.37	34.42	34.47	0.001	0.002	0.004	11.48	12.91	15.37	8.21	14.91	24.4
E	4750	72	95	121	34.12	34.16	34.22	0.006	0.009	0.013	5.58	7.73	9.59	-1.44	-1.11	1.77
F	2058	167	194	223	34.32	34.4	34.49	0.006	0.011	0.018	12.22	14.32	16.47	13.74	21.46	29.89
G	521	222	236	248	34.49	34.55	34.6	0.018	0.033	0.054	16.36	17.52	18.52	29.07	34.96	41.13
H	235	240	256	264	34.57	34.65	34.7	0.052	0.119	0.188	17.69	18.69	19.44	36.14	42.96	47.11

To sum up, according to our model results, Puddies generate significant changes with respect to the mean conditions observed in all regions, particularly large differences were found in AOU and ΔN_2O in region E. In contrast the differences in the variables ΔNO_3^- and AOU were not significant in regions A and H.

3.3 Oxygen Budget in the Puddies

The processes that contribute to the modulation of the total O_2 content are represented in the advection-diffusion equation (Eq. 1, Section 2.1). One part of the equation is associated with O_2 changes due to

https://doi.org/10.5194/egusphere-2024-1290
Preprint. Discussion started: 5 June 2024

physical processes (denoted by *PHYS*) and another part is related to the production/consumption of O_2 through biogeochemical processes (*SMS*), so we can write $\frac{\partial o_2}{\partial t} = PHYS + SMS(O_2)$. PHYS comprises horizontal advective processes (HADV = XADV + YADV), horizontal mixing (HMIX) in the *x*-*y* plane, vertical advection (VADV) and vertical mixing (VMIX) in the *z*-direction so that PHYS = HADV + VADV + HMIX + VMIX. Note that HMIX and VMIX are mainly related to small-scale (subgrid-scale processes) mixing (e.g., Pizarro-Koch et al., 2019). On the other hand, the SMS(O_2) (source minus sink processes of O_2) includes primary production, remineralization, nitrification, and zooplankton excretion (SMS(O_2) = PP + Rem + Nitrif + Exc).

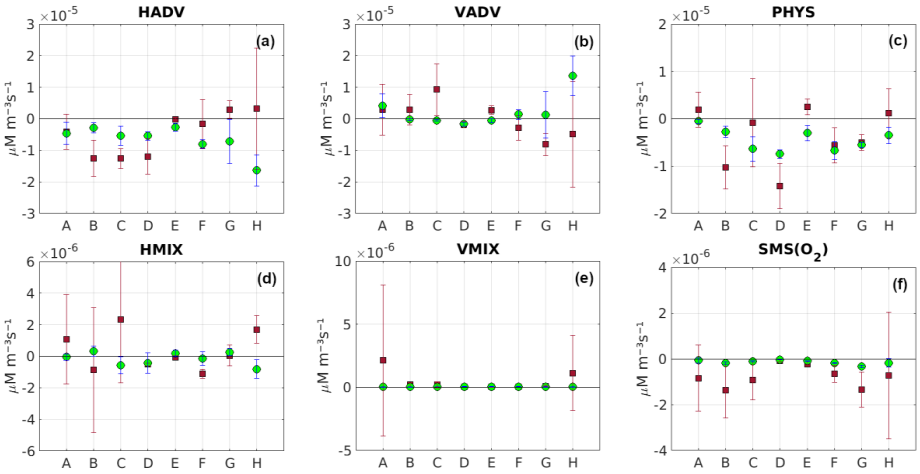

Figure 5. Mean terms involved in the O_2 budget (see equation 1). The different terms were temporally averaged inside the eddies in each subregion. PHYS is the sum of physical processes, which encompasses horizontal advection (HADV = XADV + YADV), vertical advection (VADV), horizontal mixing (HMIX), and vertical mixing (VMIX). The biogeochemical processes are included as sources minus sinks (SMS) processes impacting O_2. In particular, SMS includes the O_2 fluxes by primary production, nitrification, remineralization, and excretion of the zooplankton. Positive (negative) values indicate processes contributing to increasing (depleting) O_2 inside the eddy. A) HADV B) VADV, C) PHYS, D) HMIX, E) VMIX, and F) SMS. The averaging was conducted by dividing the eddy into 2 parts to estimate the contribution above (red squares) and below (green circles) the isopycnal surface 26.5 kg/m^3 which was asymmetric in the eddies.

We analyzed the contribution of each component of the equation to the O_2 balance in the center of the Puddies (Figure 5). Large changes in variance were observed in the upper part of the eddy cores (the skewness also changed along the vertical profile, reflecting a marked vertical variability in the probability density function of the different terms involved in the O_2 balance, Figure S4). In Figure 5, we separated the average contribution of the different terms above and below the S_{core}. Positive (negative) values indicate O_2 increasing/production (decreasing/consumption). In general, we observed that the contribution of the PHYS was negative, mainly in the lower part of the eddy, whereas there was greater variability in the upper part, with positive values dominating in some regions (A, E, and H), indicating O_2 increasing within the core (Figure 5c). On the other hand, O_2 consumption through SMS (maximum in regions B and G) occurred in the

https://doi.org/10.5194/egusphere-2024-1290
Preprint. Discussion started: 5 June 2024

upper part of the Puddies (Figure 5f). This proves that elevated biological activity is maintained in the eddies far from shore, with higher intensity in younger eddies but weakening in eddies that reach regions very distant from the coast (regions D and E). Although the SMS fluxes are on the order of O(10^{-6}), one order of magnitude lower than the PHYS of O(10^{-5}), small changes in O_2 due to SMS can also result in a sharp local spatial gradient in O_2 that induces strong changes in the advection of O_2. This could have a significant impact on the behavior of biogeochemical components that are highly sensitive to minimal changes in O_2 concentration, especially under hypoxic or suboxic conditions.

The advection components (O(10^{-5})) can be interpreted as the ability to maintain O_2 at the center of the eddy during the eddy's displacement. They dominate the O_2 budget compared to mixing processes (O(10^{-6})) involving diffusion of O_2 (Figures 5a, 5b). The lateral fluxes (HADV) showed O_2 leakage (HADV < 0) from the core mainly in the northern eddies, but not in the southern eddies (HADV > 0) where O_2 influx to the core was evident (Figure 5a). Given that VADV = $w\frac{\partial o_2}{\partial z}$, in cases where VADV < 0, it can occur in the first case where w > 0 and $\frac{\partial o_2}{\partial z}$, or a second case where w < 0 and $\frac{\partial o_2}{\partial z}$ (Figure 5b). When it occurs in the upper part of the eddy (regions F, G, and H), the first case may be more probable due to the lifting of isopycnals and the increase in O_2 to the upper part of the eddy from the core. If VADV > 0, two possibilities can occur: w > 0 and $\frac{\partial o_2}{\partial z}$ or, in the second case, w < 0 and $\frac{\partial o_2}{\partial z}$. If it occurs in the upper part of the eddy (regions A, B, C, E), the second case is more likely to be fulfilled because there is always more O_2 outside the core, indicating w < 0. On the other hand, the lower part of the eddies (regions A and H, mainly) should experience the opposite since the O_2 gradient is generally negative, then w > 0. Vertical mixing fluxes were positive in newly formed eddies (mainly in regions A and H), while lateral diffusion fluxes showed high variability in magnitude and direction (Figures 5d, 5e).

3.4 Biogeochemical evolution inside the Puddies: study cases

We considered two Puddies originated in coastal regions characterized by contrasting O_2 conditions, with one was formed in suboxic waters (i.e., O_2 < 20 µM) and the other in hypoxic waters (i.e., O_2 < 45 µM). We quantified the lifespan and transformation of the biogeochemical compounds enclosed by the eddies. The trajectories of these Puddies are shown in Figure 1b.

a) Case 1: Suboxic Puddy

The suboxic Puddy (SP) was first detected in region A (24ºS, 71.85ºW) from where it moved northwest for 420 days (~60 weeks) with an average radius of ~82 km. Its trajectory spanned between 22.36ºS and 25.32ºS and 71.85ºW and 86.53ºW, passing through regions B and C, where it disappeared (Figures 1b). In week 11, it showed a subsurface core with positive vorticity between S_{upper} and S_{core}, with velocity in the edge delimited by the r_{mean} exhibits around 10 cm s^{-1} (Figure S5a). Within the suboxic environment (O_2 < 20 µM), the puddy showed peak concentrations of NH_4^+, NO_2^- (> 0.15 µM), NO_3^- (30-40 µM), and N_2O (60 nM), and a small volume where O_2 < 1 µM (i.e., close to anoxic conditions). The maximum NO_3^- >40 µM was found in the lower part of the eddy (between 450 - 600 m depth) associated with O_2 values between 20 µM and 45 µM; the periphery showed O_2 <45 µM, and a decrease of NH_4^+, NO_2^-, and N_2O (Figures S5b, S5c, S5d).

https://doi.org/10.5194/egusphere-2024-1290
Preprint. Discussion started: 5 June 2024

SP showed a suboxic core for a year following formation (>80% of the eddy's lifespan; Figure S6), then, becoming hypoxic for the rest of its lifespan. The coefficients associated with the exponential fit for the Puddy were greater than mean state coefficients, except for O_2 where the relationship was inverse (Table 6). For the first 50 days, the biogeochemical conditions remained similar to initial conditions with positive anomalies of NO_2^-, NH_4^+, and salinity but negative anomalies of O_2, N_2O and NO_3^- (the last two at the top of the eddy). Subsequently, the largest positive anomalies in the variables occurred in the upper part of the SP above S_{core} (Figure 6). The increment in salinity after 50 days indicates intrusion of external waters (Figure 8a); however, the SMS < 0 indicated biological activity that consumes O_2 (ammonification, zooplankton excretion and nitrification), prolonging the lifespan of NO_2^- and NH_4^+ by around 6 months (see SMS term in Figure 9c, Figure 8). PHYS predominantly exhibited positive flows that increased after 100 days, where the dominant mechanisms were lateral advection (HADV; Figures 9a, 9b) as evidence for ventilation of the SP. Concentrations of NO_2^- and NH_4^+ declined with a high decay rate of k < 0.011, which is lower than the average state rate (k > 0.011; Table 6; Figures 6c, 6e, 8c, 8e). For salinity, NO_3^-, and N_2O, the decay rate was lower than that of NO_2^- and NH_4^+ because even though their concentration decreased, they were not fully depleted; however, these decreased more slowly in the SP than in the average state indicative of the capacity of the eddy to enclose and maintain the initial source waters (Table 6; Figures 6a, 6d, 6f, 8a, 8d, 8f). At the same time, O_2 had a higher rate of increase inside the SP than outside it, with rapid ventilation after 8 months (Table 6; Figures 6b, 8b).

Table 6. The salinity (g kg^{-1}), NO_3^-, NO_2^-, NH_4^+, O_2 (µM), and N_2O (nM) decay rates at the mean volume of the suboxic Puddie (SP), hypoxic Puddie (HP), and their respective mean state of the same path. It was calculated from exponential fit $y = Ae^{-kx}$, where *k* is the decay rate.

Variable	Decay rate (k)		Coefficient A		Decay rate (k)		Coefficient A	
	Suboxic Puddie (SP)	Mean state SP	SP	Mean state SP	Hypoxic Puddie (HP)	Mean state HP	HP	Mean State HP
Salinity	-7.55x10^{-6}	-1.01x10^{-5}	34.86	34.79	-7.08x10^{-6}	-2.9x10^{-6}	34.65	34.51
NO_3^-	-8.34x10^{-5}	-2.42x10^{-4}	35.95	35.87	-2.72x10^{-4}	-2.53x10^{-4}	34.71	31.21
NO_2^-	-0.0094	-0.0155	0.08	0.05	-0.007	-0.0062	0.05	0.02
NH_4^+	-0.0102	-0.0129	0.11	0.07	-0.007	-0.0057	0.11	0.05
O_2	0.0032	0.0027	12.12	25.34	0.0015	7.4x10^{-4}	53.06	102.43
N_2O	-6.88x10^{-4}	-0.0014	42.95	39.75	-7.14x10^{-4}	-6.99x10^{-4}	38.67	27.06

https://doi.org/10.5194/egusphere-2024-1290
Preprint. Discussion started: 5 June 2024

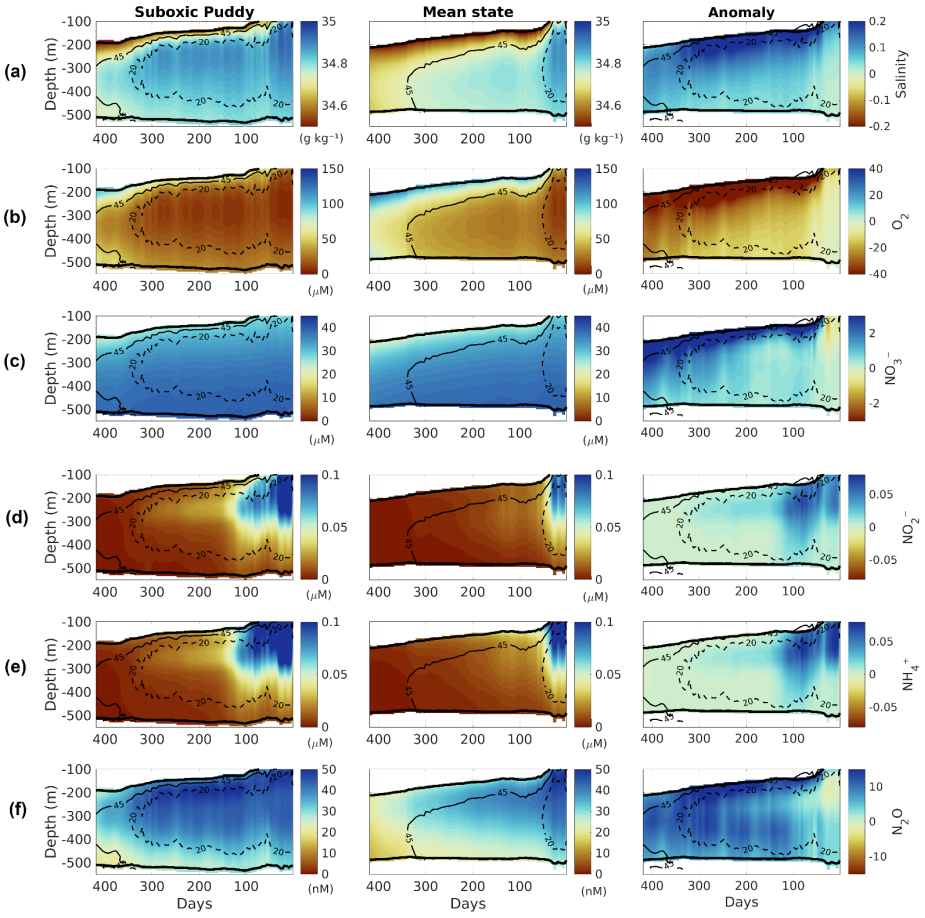

Figure 6. Vertical section of the biogeochemical components during the trajectory of the suboxic Puddy (SP) which originated in region A with a radius of 72.8 km and a lifetime of ~400 days (left boxes). The mean state (central boxes) and anomalies (right boxes) correspond to the same path of the SP. a) Absolute salinity, b) O_2, c) NO_2^-, d) N_2O, e) NH_4^+, and f) NO_3^-. The vertical section was obtained by averaging the volume of the eddy, delimited by a cylinder of its mean radius within the intrathermocline band whose boundaries are the isopycnals layers S_{upper} and S_{lower} (blue contours). Black contours show values of $O_2 < 45$ µM (solid line) and $O_2 < 20$ µM (dotted line). The trajectory of this puddy is shown in Figure 1b.

b) Case 2: Hypoxic Puddy

The Hypoxic Puddy (HP) was first observed in region G very close to the coast (36.2ºS, 74.2ºW), and its northwest trajectory lasted approximately 600 days (~86 weeks) with an average radius of 76 km. The Puddy moved within the area between 30.3ºS, 74.2ºW, and 36.9ºS, 85.3ºW, crossing through regions F and E (Figures 1b) and showing positive vorticity in the core. Concentrations of O_2 <20 µM were observed initially,

https://doi.org/10.5194/egusphere-2024-1290
Preprint. Discussion started: 5 June 2024

despite forming in an environment where generally characterized by hypoxia, and where NO_2^- (max ~0.05 μM) and N_2O (70 nM) showed maximum concentrations (Figure S5e). In the range of $20 < O_2 < 45$ μM, NO_3^- reached its maximum (35 - 38 μM) whereas other nitrogen compounds decreased (Figures S5f, S5g, S5g).

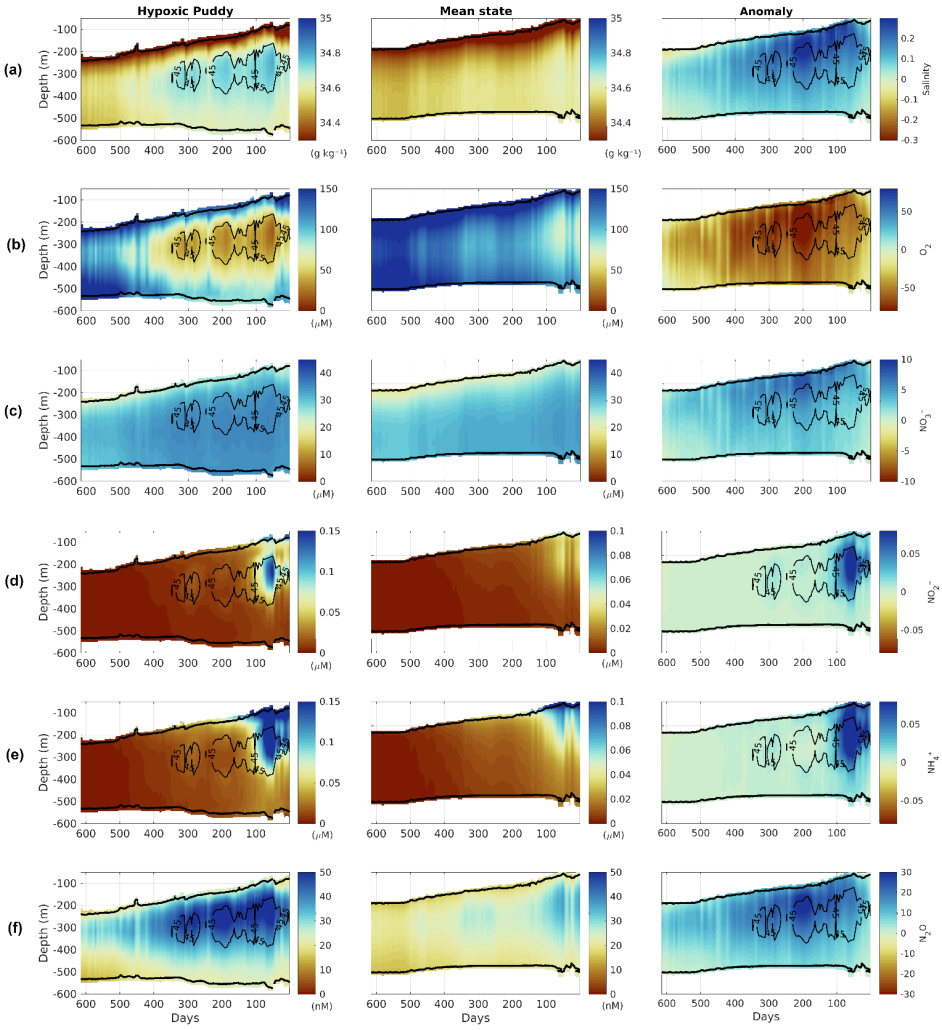

Figure 7. Same as Figure 6 but for a selected hypoxic Puddy (HP) originated in region G with a radius of 82.7 km and a lifetime of ~600 days. The trajectory is shown in Figure 1b.

The mean hypoxic condition in the core was associated with higher salinity, NO_2^-, and N_2O concentrations that persisted for >1 year (60% of the eddy's lifespan); however, on the periphery, O_2 concentrations were higher than 120 μM (Figures 7a, 7b, 7c, 7d). In the first 50 days, O_2 concentrations decreased to suboxic levels, and later to 220 days, when oxygenation was observed, O_2 levels were subsequently decreased to hypoxic range by respiration associated with biological activity (SMS < 0, Figure 9c, S6). A significant

https://doi.org/10.5194/egusphere-2024-1290
Preprint. Discussion started: 5 June 2024

contrast was observed between the properties within the HP and the average state throughout the lifespan of the eddy (Figure 7). Negative O_2 anomalies (> 50 µM), positive absolute salinity anomalies (> 0.2 g/kg), N_2O anomalies (> 20 nM), NO_3^- anomalies (> 8 µM), and NH_4^+ - NO_2^- anomalies were observed during the first 250 days (> 0.08 µM; Figure 7) when the negative SMS fluxes were greatest, indicating O_2 consumption (Figures 8 and 9c).

Simultaneously, negative PHYS fluxes were dominant where vertical advective processes occurred, although in general, the dominant mechanism controlling the O_2 balance was lateral advection, which increased positively after 300 days (Figures 8a, 8b, 9a, 9b, 9c, 9d). Horizontal and vertical mixing also supplied O_2 into the eddy during the life of the HP, but these are one or two orders of magnitude smaller than advective processes (Figures 9e, 9f).

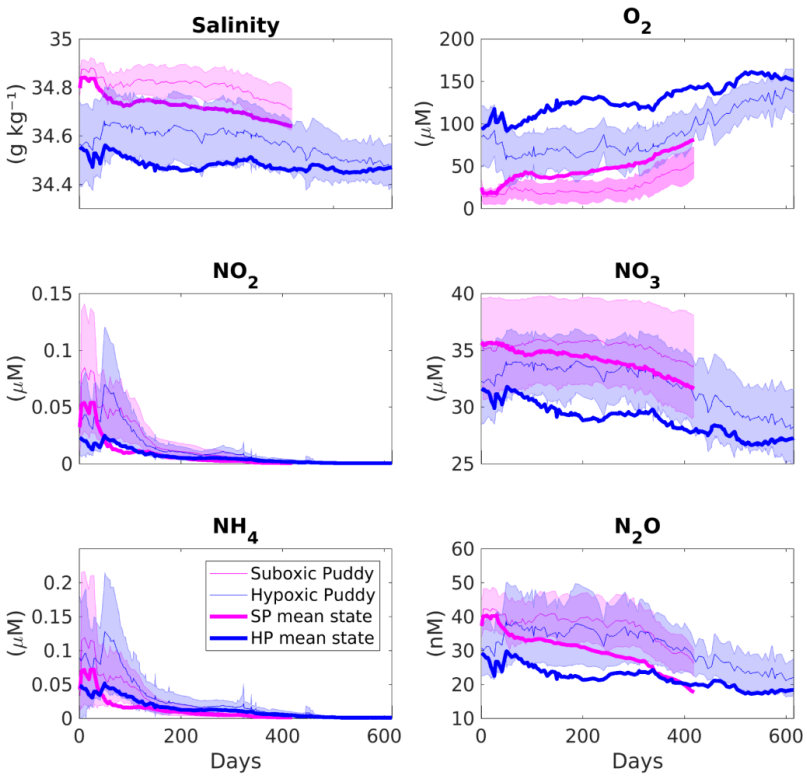

Figure 8. Comparison between the temporal evolution of the average biogeochemical properties into the suboxic (SP, magenta) and hypoxic (HP, blue) puddies shown in Figures 6 and 7. (a) Absolute salinity, (b) O_2, (c) N_2O, (d) NO_3^-, (e) NO_2^-, and (f) NH_4^+. Shading is the standard deviation indicating the range of concentration of each tracer within the eddies. Trajectories are shown in Figure 1b.

https://doi.org/10.5194/egusphere-2024-1290
Preprint. Discussion started: 5 June 2024

The coefficients A of the exponential fit for the HP and the decay rate were greater than the coefficients for the mean state (Table 6). In the case of O_2, coefficient A corresponding to the Puddy was almost half of the coefficient outside. However, the HP maintained higher biogeochemical conditions than the average state for an extended period, which may suggest that there is local production of these compounds as observed for the increase of NO_2^- and NH_4^+ concentrations after 50 days with SMS < 0 (Figure 8c, 8e, 9c).

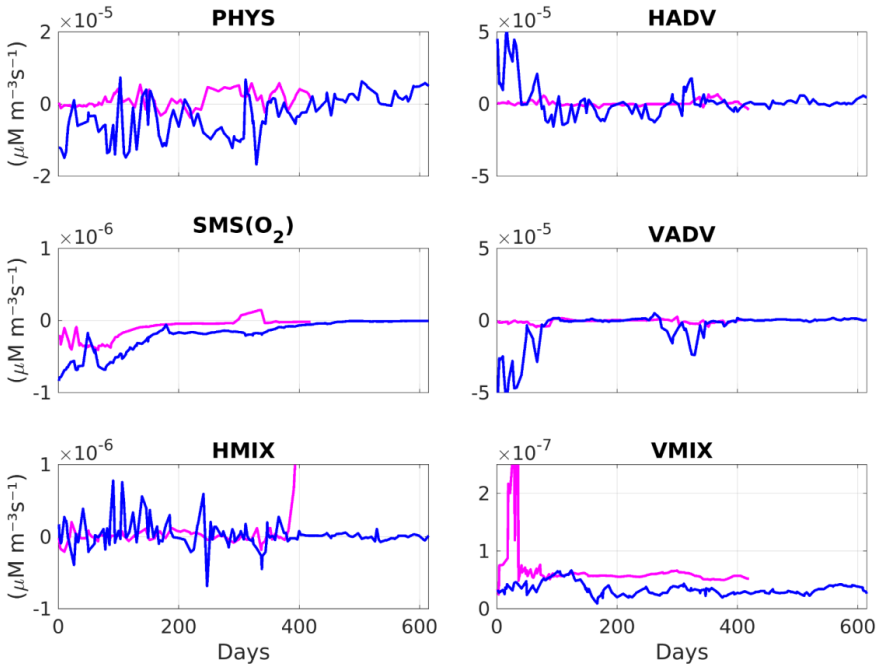

Figure 9. Comparison between the temporal evolution of the terms involved in the O_2 budget corresponding to suboxic (SP, magenta) and hypoxic (HP, blue) puddies shown in Figures 6 and 7. The terms are described in Figure 5. (a) PHYS fluxes, (b) HADV fluxes, (c) SMS fluxes, (d) VADV fluxes, (e) HMIX fluxes, and (f) VMIX fluxes.

4 Discussion

Several studies have reported on *in situ* subsurface eddies with similar biogeochemical characteristics to those observed in the present study (Stramma et al., 2013; Stramma et al., 2014; Cornejo et al., 2016; Arévalo-Martínez et al., 2016; Grundle et al., 2017; Hormazabal et al., 2013; Kartensen et al., 2017) but little detail has been presented on the recycling of bioelements within these eddies. While recent studies have used high-resolution coupled models to describe and quantify more complex processes involved in the O_2, nutrient, or organic matter balance within eddies (José et al., 2017; Frenger et al., 2018; Loveccio et al.,

https://doi.org/10.5194/egusphere-2024-1290
Preprint. Discussion started: 5 June 2024

2022), the agents generating natural variability in the lifespan of these bioelements associated with the nitrogen cycle during their trajectory from the OMZ to oceanic waters have not been analyzed in detail.

4.1 Biogeochemical anomalies in Puddies from their formation

Subsurface anticyclonic eddies appear to be formed by the separation of the Peru-Chile Undercurrent from the slope (e.g., Molemaker et al., 2015; Thomsen et al., 2016; Contreras et al., 2019). Here, we observed a higher recurrence of Puddies in certain sectors, namely, between 29º-35ºS (Figure 1c), related to the widening of the continental shelf. This change in topography may lead to greater separation of the PCUC from the slope creating favorable conditions for generation of Puddies, as previously observed by Chaigneau et al. (2009). Puddies appear to originate from instabilities forced in the bottom boundary layer at the upper continental slope – where the core of the PCUC interacts with the sea bottom (Contreras et al., 2019), and where the core of the OMZ is observed – and this source water is characterized by positive NH_4^+, NO_3^-, NO_2^- and N_2O anomalies, and very low O_2, as described in Section 3.1. However, unlike O_2 and salinity, which exhibit a more uniform gradient along the coast, several other biogeochemical components have more irregular spatial distributions depending in particular on whether conditions are hypoxic or suboxic.

In the northern part of the coastal zone, limited ventilation creates an environment with suboxic conditions and denitrification, resulting in deficits of NO_3^- and N_2O, and enrichment of NO_2^- and NH_4^+. In contrast, the central coastal waters exhibit increased NO_3^-, with the southern part showing higher N_2O concentrations. Additionally, as the formation of Puddies is associated with cross-shore velocities – exchanging nutrients between the continental shelf and open sea (Thompsen et al., 2015) – the mixture of ESSW and SAAW waters, affected also by the southward reduction of in contribution of ESSW (Silva et al., 2009), enhances the biogeochemical variability of the Puddies generated along the Chilean coast (Figure 2).

4.2 Biogeochemical Anomalies of Puddies and Mean State

In each subregion shown in Figure 1b, the Puddies resulted in positive anomalies of nutrients and low-oxygen values, and these varied with latitude. These data were summarized in Figures 3 and 4. For the tracked Puddies, HP exhibited greater anomalies during its trajectory compared to SP, even though some bioelements were found in lower concentrations in SP (Figures 6 and 7). This is related to the dominance of SAAW in the southern regions, where hypoxic Puddies are more common and contain higher O_2 concentrations and lower levels of NO_3^-, NH_4^+, NO_2^-, and N_2O than Puddies further north (Silva et al., 2009). Consequently, Puddies that capture a larger fraction of ESSW during their formation have a biogeochemical contribution nearer to the P75 (Table XX) and a larger O_2 deficit than the mean state. This suggests that the southern regions are experiencing more deoxygenation and nutrient enrichment due to the influence of Puddies than the northern regions where the OMZ is much wider.

https://doi.org/10.5194/egusphere-2024-1290
Preprint. Discussion started: 5 June 2024

4.3 Persistence of Biogeochemical Anomalies Away from the Coast

Through the case studies, we observed changes inside Puddies formed under suboxic (SP case) and hypoxic (HP case) conditions. In both cases, there was a decrease in dissolved inorganic nitrogen compounds as the Puddies aged and mixed with external waters. Similar results were observed by José et al. (2017) in the upwelling system off Peru, Frenger et al. (2018) in the four EBUS, and Loveccio et al. (2022) in the Northern Canary upwelling system. Our results indicate that Puddies have a rather permeable boundary, but the level of coherence and isolation can be important in the lifespan of compounds inside the Puddy core. The lifespan of macronutrients was similar to what was observed by Frenger et al. (2018), but in our case, N_2O, although found in minimal concentrations, has a path similar to other macronutrients like NO_3^- (Figures 6, 7). In both the SP and HP cases, NO_2^- and NH_4^+ decay rates were faster than those for NO_3^- and N_2O. Nitrate showed higher concentrations than other micronutrients, additionally, as long as there is NH_4^+ and NO_2^-, nitrification increases the NO_3^- pool in subsurface waters where it is not consumed by photosynthesis. On the other hand, the production of N_2O is a function of [NH4$^+$], [NO2$^-$], and [O_2], and depends on processes such as nitrification and denitrification. Thus, according to the parameterization of the model (see Gutknecht et al., 2013a), the part of the equation that is a function of O_2 in $SMS(N_2O)$ is calculated, for [O_2]≥1 uM, as a function of the form αe^{-O_2}. Hence, for very large values of O_2, the production of N_2O tends towards zero, and as O_2 decreases, N_2O production increases exponentially. However, this production is diminished when there is less NO_2^- and NH_4^+ available for nitrification because during denitrification, they are depleted more rapidly until the production of N_2O stops. Since the model does not consider N_2O consumption by biological processes (by denitrification or fixation), only during exchange with the atmosphere, the decrease in N_2O observed within the Puddies that move away from the coast can only be due to the physical processes involved that allow exchange with exterior waters. Therefore, Puddies are a source of this gas outward from the coast. The evidence of higher O_2 consumption during the first 100 days due to $SMS(O_2)$ suggests greater biological activity in newly formed Puddies that must be supported by dissolved organic nitrogen from the source water, as proposed by Loveccio et al. (2022). In addition, although the decay rate is higher in the HP, the SMS negative values are also higher than in the SP, which could suggest a greater local production of nutrients due to the effect of remineralization that could extend the lifetime of these elements in the HP, as we mentioned in Section 3.4. The biological activity allows low-oxygen cores to persist longer, facilitating the maintenance of $O_2 < 20$ µM in the cores of the Puddies, where denitrification processes continue, while the edges ventilate the eddy generating unique conditions. In fact, this could explain the high biogeochemical variability observed in the core of the Puddies identified in all regions, which increased the farther they were from the coast (Figure 3, 4). The eddies characterized in each subregion provide insight into how and to what extent these eddies evolved from their formation to their arrival anywhere in the SEP.

4.4 Advantages and Disadvantages of the Model for Low Oxygen Conditions

AOU:NO_3^- ratios of 250:30 (up to 20:1) have been documented in the Atlantic from *in situ* monitoring of NO_3^- within eddies (Kartensen et al., 2017), with $NO_3^- < 25$ µM observed in eddy cores with $O_2 < 5$ µM in the SEP (Stramma et al., 2013). The eddies modeled here showed AOU values similar to those found by Karstensen et al. (2017) in the eastern tropical North Atlantic, although NO_3^- was overestimated by 3 - 5 µM

https://doi.org/10.5194/egusphere-2024-1290
Preprint. Discussion started: 5 June 2024

with a ratio AOU:ΔNO_3^- of 5:1 (Figures 3b, 4b, 5c; Stramma et al., 2013). Suboxic Puddies build up NO_2^- and the maximum concentration appears underestimated in the model compared to previously reported in situ results (Stramma et al., 2013; Cornejo et al., 2012; Cornejo-D'Ottone et al., 2016). The relationship between NO_2^- and ΔN_2O in the northern zone also showed underestimation for both parameters, particularly NO_2^-. At the N_2O maximum produced by the model (>30 nM, Figure 4), field data shows NO_2^- values >1 µM (Cornejo et al., 2012), but we obtained a NO_2^- maximum of 0.15 µM (Figures 3c, 4c). Comparing our results with eddies monitored in the Southeastern Pacific, the N_2O concentrations observed in open ocean eddies agrees with those measured by Cornejo et al. (2016; Figure 3d, 7 case 1, S4) in an eddy originated in front of Concepcion (south zone), although there are differences of up to 20 nM with the eddy reported by Arévalo-Martínez et al. (2016; Figure 7, S4) in north zone of Chile. These results indicate better representation of biogeochemical processes by the model in a hypoxic than suboxic environment.

Biogeochemical components are challenging to model due to the numerous physical, biogeochemical, and biological processes involved. Specifically, under hypoxic or suboxic conditions, the nitrogen cycle is more complex due additional processes that occur within a narrow O_2 range, which increases the sensitivity of the system. Processes such as denitrification remove nitrogen from the system but generate by-products such as N_2O and NO_2^- through the alternative metabolic pathways that are less significant under oxic conditions (e.g., denitrification, NO_3^- reduction). Denitrification is a complex process to parameterize, involving a range of steps for each nitrogen component and various rates of decomposition of particulate (large and small) and dissolved material. However, despite the attempt to consider these processes realistically, the model remains an approximation, but does reasonably represent the processes involved, primarily within the intrathermocline band (see Appendix 1). In the suboxic zone, while the model underestimated O_2, NO_3^- remained overestimated, but in the subsurface band associated with the core of OMZ, the model represented the lowest biases in O_2 and nitrogen evaluated with CARS (see Appendix 1). This allowed us to present a more robust statistical analysis of biogeochemical properties inside and outside the eddies. Despite the difficulty in simulating realistically sharp mean gradients in water mass properties, the model did highlight typical features, such as NO_3^- consumption and production of NO_2^- and N_2O, processes that persist within Puddies far from their origin within the OMZ.

5 Conclusions

Using a high-resolution coupled simulation of the Southeast Pacific, we characterize the changes in internal biogeochemistry, their differences with external properties, and the processes involved in the O_2 balance of Puddies during their transport to oceanic waters. The model resolved eddy dynamics and biogeochemical processes related to the nitrogen cycle, which exhibit characteristic processes of EBUS, such as denitrification. This methodology allowed us to make a statistical approximation of the biogeochemical changes that occur within these Puddies, and the dominant mechanisms involved in modulating the concentrations of these compounds during their trajectories from the formation zone to hundreds of kilometers offshore.

https://doi.org/10.5194/egusphere-2024-1290
Preprint. Discussion started: 5 June 2024

During formation, Puddies capture the biogeochemical signal that varies according to their origin, which is associated with the core of the Peru-Chile Undercurrent. Permeability at the periphery enables exchange with external waters that modulate the original signature, however, the core signal retains certain characteristic negative anomalies of O_2 and positive anomalies of other biogeochemical tracers. These disturbances associated with Puddies may contribute to the average properties being > P90 in the open ocean, contrasting with the formation zone where it is over P50. Although a high percentage of Puddies near the coast exhibit suboxic cores (all in the north and 70% in central-south Chile), the proportion decreases with distance from the coast, where hypoxic cores become more predominant (60% in C and G regions) indicating core ventilation during their trajectory, as observed in the OMZs of the SP and HP in Section 3.4. The dominant mechanism for O_2 input or output to/from the eddy core is lateral and vertical advection, with vertical mixing supply two orders of magnitude smaller. Consumption of O_2 through biological activity was observed for around 6 - 12 months, allowing longer term persistence of low O_2 conditions in the core despite ventilation at the periphery of the Puddy. This, in turn, can sustain processes – such as denitrification, which occur under hypoxic or suboxic conditions within the OMZ – into areas far beyond the OMZ contained within niches in the core with $O_2 < 20$ μM. The southern regions experience more deoxygenation and nutrient enrichment due to the influence of Puddies than the northern regions, where the OMZ is wider, and where water mass transition occurs. Clearly, the formation of Puddies is an important process in the zonal extension of boundaries at the Southern tip of the OMZ.

Biogeochemical tracers have a variety of lifespans depending on original concentration, and rates of demand and production. Ammonium and NO_2^- tend to decline within the first 6 months, most strongly the first 100 days of the life of the eddy, while other components decrease in concentration but persist longer. Despite being produced in low concentrations, N_2O is retained in Puddies further from the coast, thus serving as a proxy of denitrification in the source water and also increasing the subsurface reservoir of this greenhouse gas in the open ocean.

Higher-resolution models allow us to characterize the mixing processes involved in eddy core ventilation and the exchange of properties with external waters by submesoscale dynamics. Coupling more complex biogeochemical models will serve to quantify the effects of other SMS processes within Puddies that are not considered in the present study. Validation and supplementary statistics of Puddies through further observations in the study area are recommended in order to deepen our understanding of coupled processes occurring in surface and subsurface eddies.

https://doi.org/10.5194/egusphere-2024-1290
Preprint. Discussion started: 5 June 2024

Appendix 1: Biogeochemical model assessment

A1.1 Data

Climatological O_2 and NO_3^- fields were taken from the CSIRO Atlas of Regional Seas (CARS2009; www.marine.csiro.au/~dunn/cars2009/) for the biogeochemical model assessment, which has a spatial resolution of 0.5 degrees for each month. For the study region, a depth of 800 m was adopted, distributed every 10 meters to the first 300 m, every 25 meters to 500 m, and then every 50 meters down to 800m.

A1.2 Model Assessment

A1.2.1 Surface Nitrate

Modeled concentrations of surface NO_3^- were compared to data from CARS. Model predictions showed low NO_3^- (< 2 µM) in general, except in the areas near the coast and in the southwest where concentrations reached 8 µM (Fig. A1a). The observed concentrations were higher, particularly in the south (Fig. A1b). Overall, the model underestimated NO_3^- concentrations in most of the domain, although the differences compared to CARS were relatively minor, ranging between 0 - 4 µM south of 30ºS and between 0-2 µM north of 30ºS (Figs. A1a, A1c). Adjacent to the coast between 25º-35ºS, the model overestimated concentrations by ~7 µM (Fig. A1c). In general, differences were minimal over most of the study area, and it can therefore be considered that the model fairly well represents surface NO_3^-.

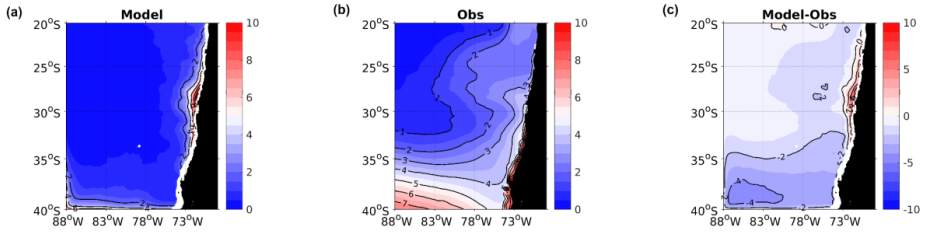

Figure A1. Spatial distribution of mean surface NO_3^-. (a) ROMS-BioEBUS simulation, (b) CARS climatology, and (c) BIAS (model - observations).

A1.2.2 Oxygen and nitrate on the isopycnal layers

Observed data from CARS were used to assess the average O_2 and NO_3^- modeled in different density layers S_{upper}, S_{lower} and S_{core} (Figures A2, A3, A4). The model captured the principal characteristics of O_2 and NO_3^-, displaying a similar structure and latitudinal and zonal gradients. Compared with observed data, lower O_2 concentrations and higher NO_3^- concentrations were predicted near the coast and north of 30ºS associated with the meridional changes of the offshore extension of the OMZ.

https://doi.org/10.5194/egusphere-2024-1290
Preprint. Discussion started: 5 June 2024

In the S_{upper} surface, observations revealed discontinuous areas with lower O_2 concentrations north of 25º S (O_2<100 µM), between 30 - 31ºS and 35 - 36º S (O_2<150 µM). The model mostly underestimated these O_2 concentrations by 40 µM north of 30º S, by around 20 µM between 30 - 35º S, and overestimated them by 20 µM between 35 - 38º S near the slope, but performed better south of 35º S offshore. For NO_3^-, observations indicated very low concentrations mainly along the coast between 23 - 35º S (<10 µM), with an increase to >15 µM in the oceanic region. Therefore, the model overestimated concentrations in the coastal zone (>10 µM) and in the northern oceanic zone (4 - 8 µM, Figures A2).

Regarding the S_{core} layer, the model performed better in the northern region, underestimating O_2 concentrations between 0 - 10 µM. Off the coast, the bias ranged from -10 to 10 µM. However, south of 30º S, between 75 - 80º W, the model overestimated O_2 concentrations by over 40 µM, whereas west of 82º W, the bias varied between -10 to 10 µM. Nitrate overestimation was observed in the coastal region with concentrations exceeding 6 - 8 µM, particularly in the northern oceanic area (2 - 4 µM). The model better reproduced real NO_3^- data in the region west of 78º W and south of 30ºS (Figure A3).

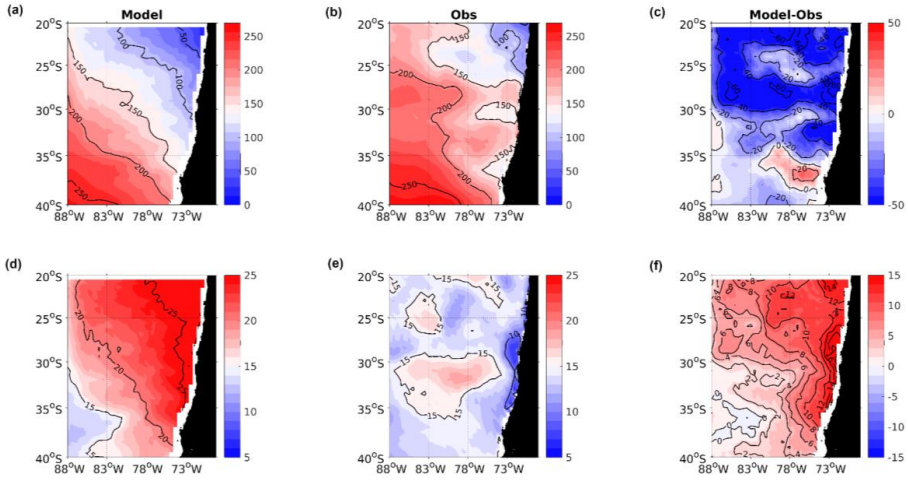

Figure A2. (a-c) Mean O_2 and (d - f) mean NO_3^- concentration in the isopycnal layer S_{upper} = 26.0 kg/m³ from the ROMS-BioEBUS simulation (left boxes), CARS climatology (middle boxes), and BIAS (right boxes).

https://doi.org/10.5194/egusphere-2024-1290
Preprint. Discussion started: 5 June 2024

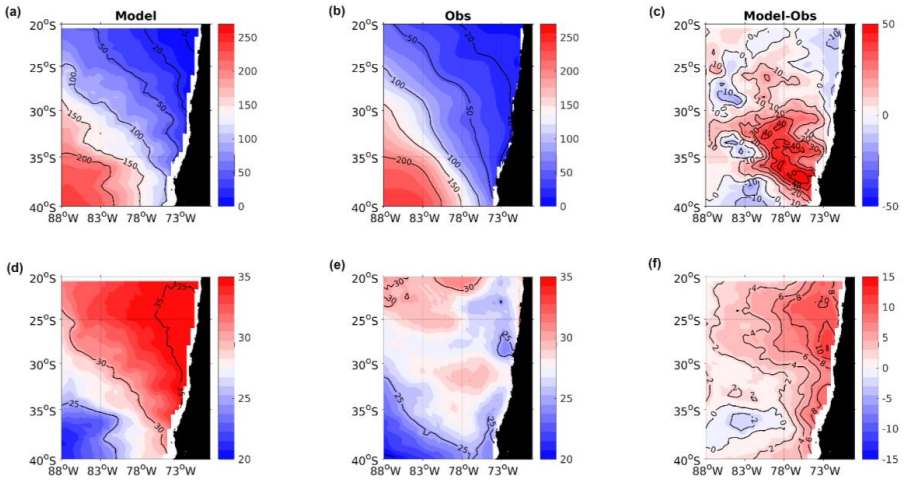

Figure A3. (a-c) Mean O_2 and (d - f) mean NO_3^- concentration in the isopycnal layer S_{core} = 26.6 kg/m³ from the ROMS-BioEBUS simulation (left boxes), CARS climatology (middle boxes), and BIAS (right boxes).

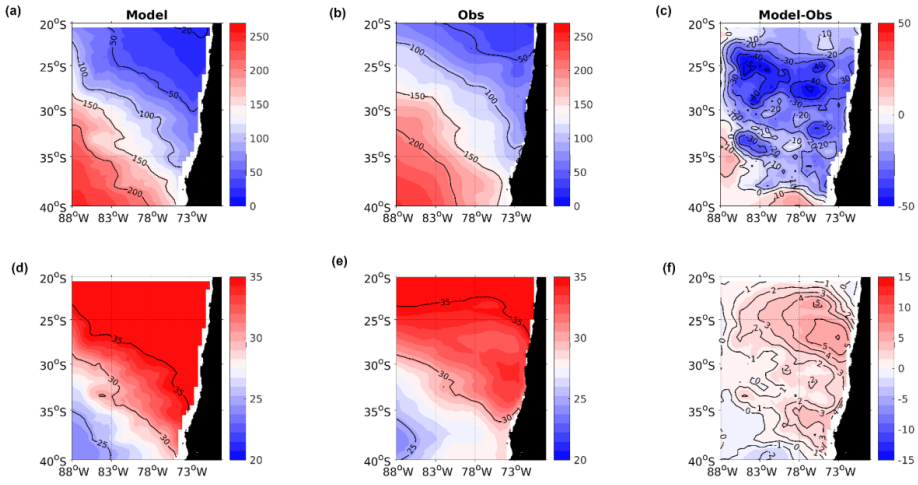

Figure A4. (a-c) Mean O_2 and (d - f) mean NO_3^- concentration in the isopycnal layer S_{lower} = 26.9 kg/m³ from the ROMS-BioEBUS simulation (left boxes), CARS climatology (middle boxes), and BIAS (right boxes).

In the S_{lower} layer, the model underestimated O_2 concentrations north of 30º S by between 10 - 40 µM, with a smaller underestimation south of 30º S (10 - 30 µM) and an overestimation in the southwest (0 - 10 µM). The model represented NO_3^- well, with deviations from observations ranging from -2 to 5 µM and with the greatest overestimation occurring in the region where $O_2 < 50$ µM (Figure A4).

https://doi.org/10.5194/egusphere-2024-1290
Preprint. Discussion started: 5 June 2024

A1.2.3 Vertical Structure

The vertical structure of O_2 and NO_3^- was evaluated by comparing the model with the CARS climatology along zonal sections at 25ºS, 30ºS, and 35ºS (Figures A5, A6). Along the latitudinal gradient, the contour of 50 µM O_2 decreased towards the south. Observations show an elongated low-oxygen tongue in subsurface waters compared to model predictions, along with an intrusion of oxygenated waters both at the surface and at depth (~600 m), enclosing the low-oxygen water with pronounced oxyclines (Figure A5). This is consistent with a greater bias within the oxyclines, where the model tended to underestimate observed data, particularly in the lower oxycline (underestimated by up to 60 µM). In the subsurface layer between 200 - 400 m, the model better represented O_2 levels, especially at 25 - 30ºS where differences ranged from 0 - 10 µM (Figure A5c, A5f). At 35ºS, there was an overestimation (40 µM) between 75-80ºW low 200 - 300 m depth (Figure A5i).

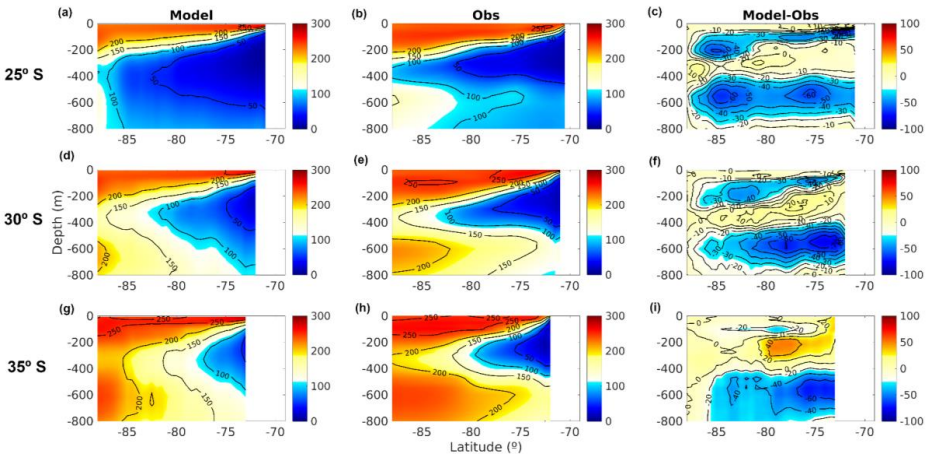

Figure A5. Zonal section of mean O_2 concentration at (a - c) 25ºS, (d - e) 30ºS, and (f - h) 35ºS. (a, d, g) from the ROMS-BioEBUS simulation (left boxes), CARS climatology (middle boxes), and BIAS (right boxes).

Along 25º S the model predicted higher subsurface NO_3^- concentrations near the coast compared to observations, showing differences of up to 15 µM. Below 400 m of depth, overestimations ranged from 0 - 4 µM (Figure A6a, A6b, A6c). These differences decreased towards the south; at 30º S and 35º S, the most significant differences extended from the coast to 76º W and below -300 m (overestimations of 8 - 12 µM), whereas elsewhere, differences remained between 0 - 4 µM. Subsurface NO_3^- was underestimated by 2 µM by the model at 35º W and west of 80º W (Figures A6f, A6i).

The Taylor diagram summarizes an annual average statistic of O_2 and NO_3^- for each of the subregions by comparing the model to the CARS climatology in the upper 800 m of the water column (Figures A7, A8). Estimates of standard deviation, correlation, and RMSE reveal that the current model configuration is generally in reasonable agreement with observations, primarily in the subsurface layer where most of the

https://doi.org/10.5194/egusphere-2024-1290
Preprint. Discussion started: 5 June 2024

properties of Puddies were computed. Therefore, there is confidence in using the model for the biogeochemical characterization of these mesoscale processes.

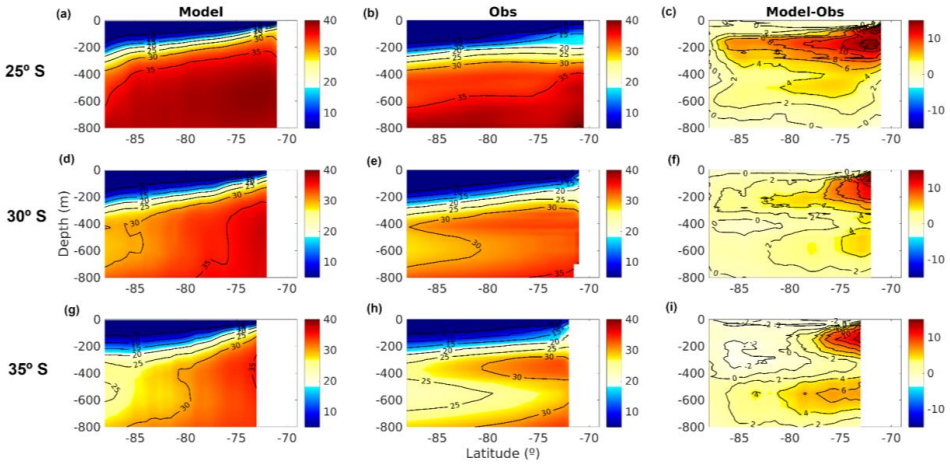

Figure A6. Zonal section of mean NO_3^- concentration at (a - c) 25ºS, (d - e) 30ºS, and (f - h) 35ºS. (a, d, g) from the ROMS-BioEBUS simulation (left boxes), CARS climatology (middle boxes), and BIAS (right boxes).

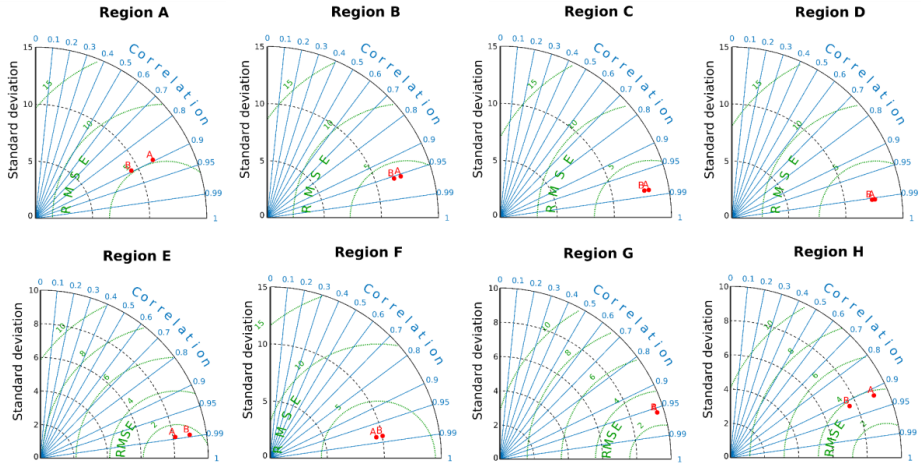

Figure A7. Annual mean Taylor diagram for O_2 concentrations in the eight subregions of the study zone (20-40 ºS, from the coast to 88ºW). The average was calculated between 800 m depth and the surface. ROMS-BioEBUS simulation (A, red circle) was compared with CARS climatology (B). The X-Y axis refers to the standard deviation (black lines), correlations in the radial axis (blue lines) and RMSE is indicated by curved lines (green).

https://doi.org/10.5194/egusphere-2024-1290
Preprint. Discussion started: 5 June 2024

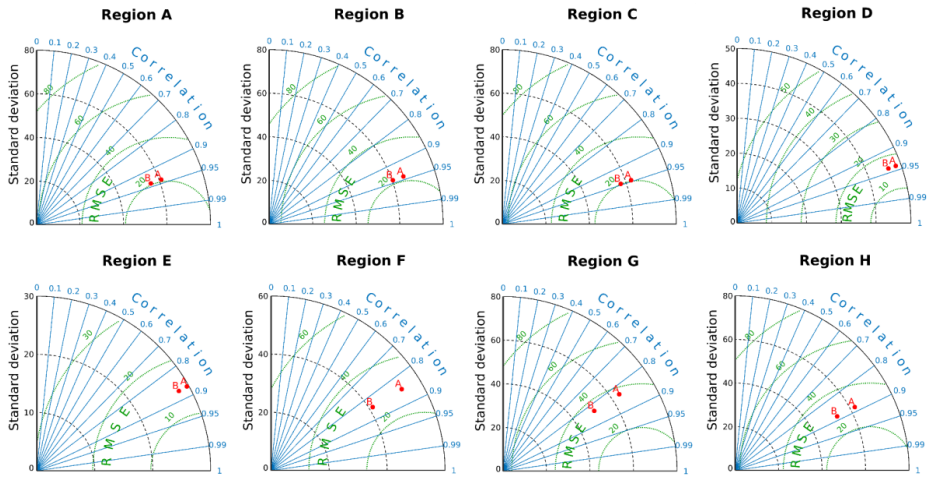

Figure A8. Annual mean Taylor diagram for NO_3^- concentrations in the eight subregions of the study zone (20-40 ºS, from the coast to 88ºW). The average was calculated for the water column between 0-800 m. ROMS-BioEBUS simulation (A, red circle) was compared with CARS climatology (B). The X-Y axis refers to the standard deviation (black lines), correlations in the radial axis (blue lines) and RMSE is indicated by curved lines (green).

Code availability

ROMS model code is available at http://www.croco- ocean.org. All input data set and configuration of our ROMS/BIOEBUS simulations are described in section and in the references therein. This work was granted access to the HPC resources of CALMIP supercomputing center at the Toulouse University under the allocations 2017-1044 and 2018- 1044.

Author contribution

LOC, OP, MC and BD designed the study. BD performed the simulation. LOC made the assessment, eddy identification and statistical analysis of the model outputs. OP supervised the project. LOC interpreted the results and wrote the manuscript with contributions from all co-authors.

Competing interests

The authors declare that they have no conflict of interest.

Acknowledgements: We thank M. Pizarro-Koch for their valuable contributions to this work. LOC was supported by ANID doctoral scholarships and the R20F0002 (PATSER) ANID program. This research was partially supported by ANID (FONDECYT projects: 1181872 & 1241203). OP thanks support from

(Millenium Institute of Oceanography grant IC-120019). Additional support was provided by the BD acknowledges support from ANID (Concurso de Fortalecimiento al Desarrollo Cientıfico de Centros Regionales 2020-R20F0008-CEAZA, Anillo Eclipse ACT210071 and Centro de Investigación Oceanográfica en el Pacífico Sur-Oriental COPAS COASTAL FB210021, Fondecyt Regular N°1190276). B.D. is was supported by the EU H2020 FutureMares project (Theme LC-CLA-06-2019, Grant agreement No 869300) and the CE2COAST project funded by ANR (FR), BELSPO (BE), FCT (PT), IZM (LV), MI (IE), MIUR (IT), Rannis (IS) and RCN (NO) through the 2019 "Joint Transnational Call on Next Generation Climate Science in Europe for Oceans" initiated by JPI Climate and JPI Oceans.

References

Altabet, M. A., Ryabenko, E., Stramma, L., Wallace, D. W., Frank, M., Grasse, P., & Lavik, G. (2012). An eddy-stimulated hotspot for fixed nitrogen-loss from the Peru oxygen minimum zone. *Biogeosciences*, *9*(12), 4897-4908.

Arévalo-Martínez, Damian L., Annette Kock, Carolin R. Löscher, Ruth A. Schmitz, Lothar Stramma, & Hermann W. Bange. 2016. "Influence of Mesoscale Eddies on the Distribution of Nitrous Oxide in the Eastern Tropical South Pacific." *Biogeosciences* 13 (4): 1105–18. https://doi.org/10.5194/bg-13-1105-2016.

Auger, P. A., Bento, J. P., Hormazabal, S., Morales, C. E., & Bustamante, A. (2021). Mesoscale variability in the boundaries of the oxygen minimum zone in the eastern South Pacific: Influence of intrathermocline eddies. Journal of Geophysical Research: Oceans, 126, e2019JC015272. https://doi.org/10.1029/2019JC015272

Bettencourt, J. H., López, C., Hernández-García, E., Montes, I., Sudre, J., Dewitte, B., et al. (2015). Boundaries of the Peruvian oxygen minimum zone shaped by coherent mesoscale dynamics. Nature Geoscience, 8(12), 937–940. https://doi.org/10.1038/ngeo2570

Chaigneau, A., Eldin, G., & Dewitte, B. (2009). Eddy activity in the four major upwelling systems from satellite altimetry (1992–2007). *Progress in Oceanography*, *83*(1-4), 117-123.

Chaigneau, A., Le Texier, M., Eldin, G., Grados, C., & Pizarro, O. (2011). Vertical structure of mesoscale eddies in the eastern South Pacific Ocean: A composite analysis from altimetry and Argo profiling floats. Journal of Geophysical Research, 116(C11), C11025. https://doi. org/10.1029/2011JC007134

Chenillat, F., Franks, P. J., & Combes, V. (2016). Biogeochemical properties of eddies in the California Current System. *Geophysical Research Letters*, *43*(11), 5812-5820.

Collins, C. A., Margolina, T., Rago, T. A., & Ivanov, L. (2013). Looping RAFOS floats in the California current system. *Deep Sea Research Part II: Topical Studies in Oceanography*, *85*, 42-61.

Combes, V., Hormazabal, S., & Di Lorenzo, E. (2015). Interannual variability of the subsurface eddy field in the Southeast Pacific. *Journal of Geophysical Research: Oceans*, *120*(7), 4907-4924.

Contreras, M., Pizarro, O., Dewitte, B., Sepulveda, H. H., & Renault, L. 2019. "Subsurface mesoscale eddy generation in the ocean off central Chile." *Journal of Geophysical Research: Oceans*. https://doi.org/10.1029/2018JC014723

Cornejo, M., L. Bravo, M. Ramos, O. Pizarro, J. Karstensen, M. Gallegos, M. Correa-Ramirez, N. Silva, L. Farias, & L. Karp-Boss. 2015. "Biogeochemical Characteristics of a Long-Lived Anticyclonic Eddy in the Eastern South Pacific Ocean." *Biogeosciences Discussions* 12 (17): 14481–506. https://doi.org/10.5194/bgd-12-14481-2015.

https://doi.org/10.5194/egusphere-2024-1290
Preprint. Discussion started: 5 June 2024

Couespel, D., Lévy, M., & Bopp, L. (2019). Major contribution of reduced upper ocean oxygen mixing to global ocean deoxygenation in an Earth system model. Geophysical Research Letters, 46(21), 12239–12249. https://doi.org/10.1029/2019GL084162

Czeschel, R., L. Stramma, R. A. Weller, & T. Fischer. 2015. "Circulation, Eddies, Oxygen, and Nutrient Changes in the Eastern Tropical South Pacific Ocean." *Ocean Science* 11 (3): 455–70. https://doi.org/10.5194/os-11-455-2015.

Dadou, I., Lamy, F., Rabouille, C., Ruiz-Pino, D., Andersen, V., Bianchi, M., & Garçon, V. (2001). An integrated biological pump model from the euphotic zone to the sediment: a 1-D application in the Northeast tropical Atlantic. *Deep Sea Research Part II: Topical Studies in Oceanography*, *48*(10), 2345-2381.

Dewitte, B., Vazquez-Cuervo, J., Goubanova, K., Illig, S., Takahashi, K., Cambon, G., ... & Ortlieb, L. 2012. "Change in El Niño flavours over 1958–2008: Implications for the long-term trend of the upwelling off Peru." *Deep Sea Research Part II: Topical Studies in Oceanography*, *77*, 143-156.

Dugan, J. P., R. P. Mied, P. C. Mignerey, & A. F. Schuetz. 1982. "Compact, Intrathermocline Eddies in the Sargasso Sea." *Journal of Geophysical Research* 87 (C1): 385–93. https://doi.org/10.1029/JC087iC01p00385.

Faghmous, J. H., Frenger, I., Yao, Y., Warmka, R., Lindell, A., & Kumar, V. (2015). A daily global mesoscale ocean eddy dataset from satellite altimetry. *Scientific data*, *2*(1), 1-16.

Faghmous, J. H. et al. 2015. "A daily global mesoscale ocean eddy dataset from satellite altimetry." *Sci. Data* 2:150028 doi: 10.1038/sdata.2015.28.

Fauzi, R., Mantoura, C., Law, C. S., Owens, N. J., Burkill, P. H., Woodward, E. M. S., ... & Llewellyn, C. A. (1993). Nitrogen biogeochemical cycling in the northwestern Indian Ocean. *Deep Sea Research Part II: Topical Studies in Oceanography*, *40*(3), 651-671.

Frenger, Ivy, Daniele Bianchi, Carolin Stührenberg, Andreas Oschlies, John Dunne, Curtis Deutsch, Eric Galbraith, & Florian Schütte. 2018. "Biogeochemical Role of Subsurface Coherent Eddies in the Ocean: Tracer Cannonballs, Hypoxic Storms, and Microbial Stewpots?" *Global Biogeochemical Cycles* 32 (2): 226–49. https://doi.org/10.1002/2017GB005743.

Garcia, H. E., & Gordon, L. I. (1992). Oxygen solubility in seawater: Better fitting equations. *Limnology and oceanography*, *37*(6), 1307-1312.

Goreau, T. J., Kaplan, W. A., Wofsy, S. C., McElroy, M. B., Valois, F. W., & Watson, S. W. (1980). Production of NO_2^- and N_2O by nitrifying bacteria at reduced concentrations of oxygen. *Applied and environmental microbiology*, *40*(3), 526-532.

Goubanova, K., Echevin, V., Dewitte, B., Codron, F., Takahashi, K., Terray, P., & Vrac, M. (2011). Statistical downscaling of sea-surface wind over the Peru–Chile upwelling region: diagnosing the impact of climate change from the IPSL-CM4 model. *Climate Dynamics*, *36*, 1365-1378.

Grados, D., Bertrand, A., Colas, F., Echevin, V., Chaigneau, A., Gutiérrez, D., et al. (2016). Spatial and seasonal patterns of fine-scale to mesoscale upper ocean dynamics in an Eastern Boundary Current System. Progress in Oceanography, 142, 105–116. https://doi. org/10.1016/j.pocean.2016.02.002

Grundle, D. S., C. R. Löscher, G. Krahmann, M. A. Altabet, H. W. Bange, J. Karstensen, A. Körtzinger, & B. Fiedler. 2017. "Low Oxygen Eddies in the Eastern Tropical North Atlantic: Implications for N_2O Cycling." *Scientific Reports* 7 (1): 1–10. https://doi.org/10.1038/s41598-017-04745-y.

Gutknecht, E., Dadou, I., Le Vu, B., Cambon, G., Sudre, J., Garçon, V., E. Machu, T. Rixen, A. Kock, A. Flohr, & Paulmier, A. 2013a. "Coupled physical/biogeochemical modeling including O2-dependent processes in the Eastern Boundary Upwelling Systems: application in the Benguela." *Biogeosciences*, 10(6), 3559-3591.

https://doi.org/10.5194/egusphere-2024-1290
Preprint. Discussion started: 5 June 2024

Helly, J. J., & Levin, L. A. (2004). Global distribution of naturally occurring marine hypoxia on continental margins. Deep Sea Research Part I: Oceanographic Research Papers, 51, 1159–1168. https://doi.org/10.1016/j.dsr.2004.03.009

Hormazabal, Samuel. 2004. "Coastal Transition Zone off Chile." *Journal of Geophysical Research* 109 (C1): C01021. https://doi.org/10.1029/2003JC001956.

Hormazabal, Samuel, Vincent Combes, Carmen E. Morales, Marco A. Correa-Ramirez, Emmanuel Di Lorenzo, & Sergio Nuñez. 2013. "Intrathermocline Eddies in the Coastal Transition Zone off Central Chile (31-41°S)." *Journal of Geophysical Research: Oceans* 118 (10): 4811–21. https://doi.org/10.1002/jgrc.20337.

Huret, M., Dadou, I., Dumas, F., Lazure, P., & Garçon, V. (2005). Coupling physical and biogeochemical processes in the Rio de la Plata plume. *Continental Shelf Research*, *25*(5-6), 629-653.

Johnson, G. C., & McTaggart, K. E. (2010). Equatorial Pacific 13 C water eddies in the eastern subtropical South Pacific Ocean. *Journal of Physical Oceanography*, *40*(1), 226-236.

Jose, Y. S., Aumont, O., Machu, E., Penven, P., Moloney, C. L., & Maury, O. (2014). Influence of mesoscale eddies on biological production in the Mozambique Channel: Several contrasted examples from a coupled ocean-biogeochemistry model. *Deep Sea Research Part II: Topical Studies in Oceanography*, *100*, 79-93.

José, Y. S., Dietze, H., & Oschlies, A. (2017). Linking diverse nutrient patterns to different water masses within anticyclonic eddies in the upwelling system off Peru. *Biogeosciences*, *14*(6), 1349-1364.

Karstensen, J., B. Fiedler, F. Schütte, P. Brandt, A. Körtzinger, G. Fischer, R. Zantopp, J. Hahn, M. Visbeck, & D. Wallace. 2015. "Open Ocean Dead Zones in the Tropical North Atlantic Ocean." *Biogeosciences* 12 (8): 2597–2605. https://doi.org/10.5194/bg-12-2597-2015.

Karstensen, J., Schütte, F., Pietri, A., Krahmann, G., Fiedler, B., Grundle, D., ... & Visbeck, M. (2017). Upwelling and isolation in oxygen-depleted anticyclonic modewater eddies and implications for nitrate cycling. *Biogeosciences*, *14*(8), 2167-2181.

Karstensen, J., Stramma, L., & Visbeck, M. (2008). Oxygen minimum zones in the eastern tropical Atlantic and Pacific oceans. Progress in Oceanography, 77, 331–350. https://doi.org/10.1016/j.pocean.2007.05.009

Keeling, R. F., Körtzinger, A., & Gruber, N. (2010). Ocean deoxygenation in a warming world. Annual Review of Marine Science, 2(1), 199–229. https://doi.org/10.1146/annurev.marine.010908.163855

Koné, N. V., Machu, E., Penven, P., Andersen, V., Garçon, V., Fréon, P., & Demarcq, H. (2005). Modeling the primary and secondary productions of the southern Benguela upwelling system: A comparative study through two biogeochemical models. *Global Biogeochemical Cycles*, *19*(4).

Kostianoy, A. G., & I. M. Belkin. 1989. "A Survey of Observations on Intrathermocline Eddies in the World Ocean." *Elsevier Oceanography Series* 50 (C): 821–41. https://doi.org/10.1016/S0422-9894(08)70223-X.

Lam, Phyllis, Gaute Lavik, Marlene M. Jensen, Jack van de Vossenberg, Markus Schmid, Dagmar Woebken, Dimitri Gutiérrez, Rudolf Amann, Mike S. M. Jetten, & Marcel M. M. Kuypers. 2009. "Revising the Nitrogen Cycle in the Peruvian Oxygen Minimum Zone." *Proceedings of the National Academy of Sciences* 106 (12): 4752–57. https://doi.org/10.1073/PNAS.0812444106.

Llanillo, P. J., Pelegrí, J. L., Gasser, M., Emelianov, M., Gourrion, J., Rodríguez-Santana, A., & Duarte, C. M. (2012). Meridional and zonal changes in water properties along the continental slope off central and northern Chile. *Ciencias Marinas*, *38*(1B), 307-332.

Löscher, C. R., Fischer, M. A., Neulinger, S. C., Fiedler, B., Philippi, M., Schütte, F., ... & Schmitz, R. A. (2015). Hidden biosphere in an oxygen-deficient Atlantic open-ocean eddy: future implications of ocean deoxygenation on primary production in the eastern tropical North Atlantic. *Biogeosciences*, *12*(24), 7467-7482.

https://doi.org/10.5194/egusphere-2024-1290
Preprint. Discussion started: 5 June 2024

Lovecchio, E., Gruber, N., Münnich, M., & Frenger, I. (2022). On the processes sustaining biological production in the offshore propagating eddies of the northern Canary Upwelling System. *Journal of Geophysical Research: Oceans*, *127*(2), e2021JC017691.

Fauzi, R., Mantoura, C., Law, C. S., Owens, N. J., Burkill, P. H., Woodward, E. M. S., ... & Llewellyn, C. A. (1993). Nitrogen biogeochemical cycling in the northwestern Indian Ocean. *Deep Sea Research Part II: Topical Studies in Oceanography*, *40*(3), 651-671.

Marshall, D. P., & Tansley, C. E. (2001). An implicit formula for boundary current separation. Journal of physical oceanography, 31(6), 1633-1638.

Matear, R. J., & Hirst, A. C. (2003). Long-term changes in dissolved oxygen concentrations in the ocean caused by protracted global warming. Global Biogeochemical Cycles, 17(4), 1125. https://doi.org/10.1029/2002GB001997

Mcwilliams, James C. 1985. *Submesoescale, coherent vortices in the ocean. Reviews of Geophysics* 23(2): 165-182.

Molemaker, M. Jeroen, James C. McWilliams, & William K. Dewar. 2015. "Submesoscale Instability and Generation of Mesoscale Anticyclones near a Separation of the California Undercurrent." *Journal of Physical Oceanography* 45 (3): 613–29. https://doi.org/10.1175/JPO-D-13-0225.1.

Montes, I., Dewitte, B., Gutknecht, E., Paulmier, A., Dadou, I., Oschlies, A., & Garçon, V. (2014). High-resolution modeling of the Eastern Tropical Pacific oxygen minimum zone: Sensitivity to the tropical oceanic circulation. *Journal of Geophysical Research: Oceans*, *119*(8), 5515-5532.

Morales, C. E., Hormazabal, S., Correa-Ramirez, M., Pizarro, O., Silva, N., Fernandez, C., ... & Torreblanca, M. L. (2012). Mesoscale variability and nutrient–phytoplankton distributions off central-southern Chile during the upwelling season: The influence of mesoscale eddies. *Progress in Oceanography*, *104*, 17-29.

Morel, A., & Berthon, J. F. (1989). Surface pigments, algal biomass profiles, and potential production of the euphotic layer: Relationships reinvestigated in view of remote-sensing applications. *Limnology and oceanography*, *34*(8), 1545-1562.

Naqvi, S. W. A., Bange, H. W., Farías, L., Monteiro, P. M. S., Scranton, M. I., & Zhang, J. (2010). Marine hypoxia/anoxia as a source of CH 4 and N 2 O. *Biogeosciences*, *7*(7), 2159-2190.

Oschlies, A., Brandt, P., Stramma, L., & Schmidtko, S. (2018). Drivers and mechanisms of ocean deoxygenation. Nature Geoscience, 11(7), 467–473. https://doi.org/10.1038/s41561-018-0152-2

Paulmier, A., Ruiz-Pino, D., Garçon, V., & Farias, L. (2006). Maintaining of the East South Pacific Oxygen Minimum Zone (OMZ) off Chile. Geophysical Research Letters, 33, L20601. https://doi.org/10.1029/2006GL026801

Pegliasco, Cori, Alexis Chaigneau, & Rosemary Morrow. 2015. "Main Eddy Vertical Structures Observed in the Four Major Eastern Boundary Upwelling Systems." *Journal of Geophysical Research: Oceans* 120 (9): 6008–33. https://doi.org/10.1002/2015JC010950.

Pena, M. A., Katsev, S., Oguz, T., & Gilbert, D. (2010). Modeling dissolved oxygen dynamics and hypoxia. *Biogeosciences*, *7*(3), 933-957.

Pizarro-Koch, M., Pizarro, O., Dewitte, B., Montes, I., Ramos, M., Paulmier, A., & Garçon, V. (2019). Seasonal variability of the southern tip of the Oxygen Minimum Zone in the eastern South Pacific (30-38 S): A modeling study. *Journal of Geophysical Research: Oceans*, *124*(12), 8574-8604.

Sarmiento, J. L., & Gruber, N. (2002). Sinks for anthropogenic carbon. *Physics today*, *55*(8), 30-36.

Sarmiento, J. L. (2006). *Ocean biogeochemical dynamics*. Princeton university press.

https://doi.org/10.5194/egusphere-2024-1290
Preprint. Discussion started: 5 June 2024

Schütte, F., Brandt, P., & Karstensen, J. (2016). Occurrence and characteristics of mesoscale eddies in the tropical northeastern Atlantic Ocean. *Ocean Science*, *12*(3), 663-685.

Shchepetkin, A. F., & McWilliams, J. C. (2005). The regional oceanic modeling system (ROMS): a split-explicit, free-surface, topography-following-coordinate oceanic model. *Ocean modelling*, *9*(4), 347-404.

Schmidtko, S., Stramma, L. & Visbeck, M. Decline in global oceanic oxygen content during the past five decades. *Nature* **542**, 335–339 (2017). https://doi.org/10.1038/nature21399

Smith, R. D., Dukowicz, J. K., & Malone, R. C. (1992). Parallel ocean general circulation modeling. *Physica D: Nonlinear Phenomena*, *60*(1-4), 38-61.

Stramma, L., H. W. Bange, R. Czeschel, A. Lorenzo, & M. Frank. 2013. "On the Role of Mesoscale Eddies for the Biological Productivity and Biogeochemistry in the Eastern Tropical Pacific Ocean off Peru." *Biogeosciences* 10 (11): 7293–7306. https://doi.org/10.5194/bg-10-7293-2013.

Stramma, Lothar, Robert Weller, Rena Czeschel, & Sebastien Bigorre. 2014. "Eddies and an Extreme Water mass Anomaly Observed in the Eastern South Pacific at the Stratus mooring." *Journal of Geophysical Research: Oceans* 118: 3114–27. https://doi.org/10.1002/jgrc.20224.

Stramma, L., Schmidtko, S., Levin, L. A., & Johnson, G. C. (2010). Ocean oxygen minima expansions and their biological impacts. Deep Sea Research Part I: Oceanographic Research Papers, 57, 587–595. https://doi.org/10.1016/j.dsr.2010.01.005

Suntharalingam, P., Sarmiento, J. L., & Toggweiler, J. R. (2000). Global significance of nitrous-oxide production and transport from oceanic low-oxygen zones: A modeling study. *Global Biogeochemical Cycles*, *14*(4), 1353-1370.

Suntharalingam, P., Buitenhuis, E., Le Quéré, C., Dentener, F., Nevison, C., Butler, J. H., ... & Forster, G. (2012). Quantifying the impact of anthropogenic nitrogen deposition on oceanic nitrous oxide. *Geophysical Research Letters*, *39*(7).

Thomsen, S., Kanzow, T., Krahmann, G., Greatbatch, R. J., Dengler, M., & Lavik, G. (2016). The formation of a subsurface anticyclonic eddy in the Peru-Chile Undercurrent and its impact on the near-coastal salinity, oxygen, and nutrient distributions. *Journal of Geophysical Research: Oceans*, *121*(1), 476-501.

Ulloa, O., Canfield, D. E., DeLong, E. F., Letelier, R. M., & Stewart, F. J. (2012). Microbial oceanography of anoxic oxygen minimum zones. Proceedings of the National Academy of Sciences, 109(40), 15996–16003. https://doi.org/10.1073/pnas.1205009109

Vergara, O., Dewitte, B., Montes, I., Garçon, V., Ramos, M., Paulmier, A., & Pizarro, O. (2016). Seasonal variability of the oxygen minimum zone off Peru in a high-resolution regional coupled model. *Biogeosciences*, *13*(15), 4389-4410.

Wright, Jody J., Kishori M. Konwar, & Steven J. Hallam. 2012. "Microbial Ecology of Expanding Oxygen Minimum Zones." *Nature Reviews Microbiology* 10 (6): 381–94. https://doi.org/10.1038/nrmicro2778.

Wyrtki, K. (1962), The oxygen minima in relation to ocean circulation, Deep Sea Res. Oceanogr. Abstr., 9, 11–23.

Yakushev, E. V., Pollehne, F., Jost, G., Kuznetsov, I., Schneider, B., & Umlauf, L. (2007). Analysis of the water column oxic/anoxic interface in the Black and Baltic seas with a numerical model. *Marine Chemistry*, *107*(3), 388-410.